Hindawi
Journal of Engineering
Volume 2024, Article ID 8419540, 24 pages
https://doi.org/10.1155/2024/8419540

Research Article

Brain Tumor Detection and Classification Using IFF-FLICM Segmentation and Optimized ELM Model

Suvashisa Dash,[1] Mohammed Siddique,[1] Satyasis Mishra,[2] Demissie J. Gelmecha,[2] Sunita Satapathy,[3] Davinder Singh Rathee,[2] and Ram Sewak Singh[2]

[1]*Department of Mathematics, Centurion University of Technology and Management, Bhubaneswar, Odisha, India*
[2]*Department of ECE, Adama Science and Technology University, Adama, Ethiopia*
[3]*Department of Zoology, Centurion University of Technology and Management, Bhubaneswar, Odisha, India*

Correspondence should be addressed to Satyasis Mishra; satyasismishra@gmail.com

Received 17 January 2023; Revised 30 December 2023; Accepted 6 January 2024; Published 29 January 2024

Academic Editor: Himadri Majumder

Brain cancer deaths are significantly increased in all categories of aged persons due to the abnormal growth of brain tumor tissues in the brain. The death rate can be controlled by accurate early stage brain tumor diagnosis. The detection and classification of brain tumors play a crucial role in early diagnosis and treatment planning. Brain tumor detection and classification have become challenging and time-consuming for domain-specific radiologists and pathologists in medical image analysis. So, automatic detection and classification are essential to reduce the time of diagnosis. In recent years, machine learning classifiers have played an essential role in automatically classifying brain tumors. In this research, an approach based on an improved fuzzy factor fuzzy local information C means (IFF-FLICM) segmentation and hybrid modified harmony search and sine cosine algorithm (MHS-SCA) optimized extreme learning machine (ELM) is proposed for brain tumor detection and classification. The IFF-FLICM algorithm is utilized to accurately segment the brain's magnetic resonance (MR) images to identify the tumor regions. The Mexican hat wavelet transform is employed for feature extraction from the segmented images. The extracted features from the segmented regions are fed into the MHS-SCA-ELM classifier for classification. The MHS-SCA is proposed to optimize the weights of the ELM model to improve the classification performance. Five distinct multimodal and unimodal benchmark functions are considered for optimization to demonstrate the robustness of the proposed MHS-SCA optimization technique. The image Dataset-255 is considered for this study. The quality measures such as SSIM and PSNR are considered for segmentation. The proposed IFF-FLICM segmentation achieved a peak signal-to-noise ratio (PSNR) of 37.24 dB and a structural similarity index (SSIM) of 0.9823. The proposed MHS-SCA-based ELM model achieved a sensitivity, specificity, and accuracy of 98.78%, 99.23%, and 99.12%. The classification performance results of the proposed MHS-SCA-ELM model are compared with MHS-ELM, SCA-ELM, and PSO-ELM models, and the comparison results are presented.

1. Introduction

Brain tumor detection and classification from MRI images have become an essential part of the diagnostic systems in the medical domain. The mortality rate grows abnormally due to brain tumors in the human brain. The early detection and diagnosis of brain tumors have become difficult due to the ignorance of human physiology. The brain tumor is a chronic brain disease characterized by repeated edges. Brain cancer is a complex and varied disease, and statistics can vary widely depending on factors such as the type of tumor, its location, and the patient's age, race, and other demographic characteristics. According to the American Brain Tumor Association (ABTA) [1], 80000 cases were reported where malignant brain tumors impact children and young people. Additional molecular features and updated pathologic diagnoses have even been added to the recently released 5th edition of the "World Health Organization Classification of Tumors of the Central Nervous System" in May 2021. Clinical doctors face a difficult task because of the

intricate nature of tumor diagnosis. Since manual detection cannot transform the image to the required simplified state, we provide a platform for automatically diagnosing and classifying brain tumors from magnetic resonance imaging. Therefore, early tumor detection and identification are crucial to reducing tumor-related fatalities. The classification of brain tumors is also crucial to understanding the different forms of tumors that can exist in the brain. Doctors may watch and forecast the uncontrollable expansion of cancer-affected areas at different levels by using segmentation and classification techniques, enabling appropriate early stage diagnosis.

Image segmentation from magnetic resonance imaging is a crucial and challenging undertaking to identify the tissues of brain tumors. Due to the involute structure and visual differences, it becomes a complex process. For the purpose of segmentation, FCM-based techniques were developed such as EnFCM [2], FCM_S1, FCM_S2 [2], and FGFCM [3]. However, these techniques failed due to the low noise reduction capabilities. An improved fuzzy factor-based FLICM algorithm is proposed to improve noise reduction capabilities and segmentation performance. Metaheuristic algorithms play a vital role in field optimization problems. The metaheuristic algorithm, the improvisational technique musicians use, is imitated by harmony search (HS) [4], which has received much attention. In order to achieve a better harmonic state during the process of musical improvisation, musicians constantly modify the pitch of their instruments. This is where the population-based metaheuristic technique HS is inspired [5]. The different algorithms based on harmony search, such as piecewise opposition harmony search (POHS) [6], fuzzy adaptation of parameters in harmony search (FHS) [7], improved harmony search algorithm [8], and "hybrid harmony search and particle swarm optimization algorithm (HSPSO)" [9], were developed to improve the optimization capability of the harmony search algorithm. The harmony search algorithm has better optimization capability than the variants of the algorithm. However, the HS algorithm needs support of parameter variation, structural adjustment, and hybridization with other algorithms to improve the performance. The researchers proposed different machine learning models but failed to achieve good classification performance regarding accuracy and computational time. Motivated by the advantages of machine learning and to improve the performance of the machine learning classifiers, a novel hybrid modified harmony search and sine cosine algorithm (MHS-SCA) optimization-based extreme learning machine (ELM) model is proposed for the automatic classification of brain tumors. Considering the parameter adjustment, pitch adjustment, and structural adjustment, we are motivated to propose a novel hybrid modified harmony search-sine cosine algorithm for weight optimization of ELM machine learning classifier to classify brain tumors from the MRI images. The literature review found that the MHS-SCA weight optimization of the ELM model has just been reported.

The following are the research's contributions:

(i) We have developed the mathematical algorithm of modified harmonic search-sine cosine algorithm (MHS-SCA) hybrid optimization algorithm by considering the parameters of harmony search and sine cosine algorithm.

(ii) Five benchmark functions are utilized to validate the authenticity of the modified harmonic search-sine cosine algorithm. The benchmark functions are optimized through MHS, SCA, and PSO algorithms and compared with the proposed MHS-SCA optimization technique.

(iii) We have utilized the proposed MHS-SCA for the weight optimization of the ELM classifier to improve its performance.

(iv) An improved fuzzy factor-based FLICM segmentation is proposed to detect brain tumors from MRI images.

The article is organized as follows: Section 2 presents the related work, Section 3 presents the research methodology and hybrid MHS-SCA-based ELM model explanation, Section 4 presents the benchmark validation, segmentation, and classification results, Section 5 presents a discussion of the results, and Section 6 presents conclusion followed by the references. Table 1 shows the abbreviations used in this article.

2. Related Work

Due to the mathematical complexity, FCM-based approaches could improve in reducing noise and detecting tumors in brain MRI images. To reduce the computational complexity demands caused by the spatial term, Szilagyi et al. [2] presented the enhanced FCM method (EnFCM), which uses gray levels with a smaller value than the image size. The parameter (adjustable) in EnFCM is crucial for enhancing segmentation outcomes. Although Cai and Chen's fast generalized FCM approach (FGFCM) requires more parameters than the EnFCM to ensure the segmentation's fidelity to detail and minimize noise, it increases FCM's robustness through a similarity measure factor. The membership partition matrix is subjected to median filtering in FRFCM [10] to lessen noise and increase segmentation precision. To improve the segmentation performance, we have developed an improved fuzzy factor-based fuzzy local information C means (FLICM) segmentation technique for the detection of brain tumor. Furthermore, the classification of brain tumors is important for medical practitioners. Lesion enhancement, feature extraction, selection, and classification approaches were all combined into one detection method by Amin et al. [11]. The input image was normalized using the N4ITK3 approach during the in-lesion enhancement step. Features were extracted using the histogram-oriented gradient (HOG), and their fusion was carried out using SFTA and LBP (texture-based) features.

Table 1: Abbreviations used in the article.

Abbreviations	Full form
ABTA	American Brain Tumor Association
MRI	Magnetic resonance imaging
FCM	Fuzzy C means
EnFCM	Enhanced FCM method
FCM_S1	FCM algorithm with spatial constraints (1st variant)
FCM_S2	FCM algorithm with spatial constraints (2nd variant)
NDFCM	Adaptive FCM algorithm based on noise detection
FGFCM	Fast generalized FCM
FLICM	Fuzzy local information *C* means
IFF-FLICM	Improved fuzzy factor-based fuzzy local information *C* means
FRFCM	Fast and robust FCM
HS	Harmony search
HM	Harmony memory
SCA	Sine cosine algorithm
MHS	Modified harmony search
BHS	Binary harmony search
POHS	Piecewise opposition harmony search
HSPSO	Harmony search and particle swarm optimization algorithm
HHS	Hybrid harmony search
PAR	Pitch adjusting rate
HMCR	Harmony memory consideration rate
AC-DPHS	Autonomous clustering dynamic parameter harmony search
SAMOHS	Self-adaptive multiobjective harmony search
SCCs	Strongly connected components
GLCM	Gray-level co-occurrence matrix
LBP	Local binary pattern
BPS	Bit-plane slicing
LLE	Locally linear embedding
LDA	Linear discriminant analysis
FAWT	Flexible analytical wavelet transform
DT	Decision tree
HHOCNN	Harris hawks optimized convolution network
PSO	Particle swarm optimization
MSCA-APSO	Modified sine cosine algorithm-accelerated particle swarm optimization
ELM	Extreme learning machine
SCA-ELM	Sine cosine algorithm-extreme learning machine
MHS-ELM	Modified harmony search-extreme learning machine
PSO-ELM	Particle swarm optimization-extreme learning machine
MHS-SCA-ELM	Modified harmony search-sine cosine algorithm-extreme learning machine
LLRBFNN	Local linear radial basis function neural network
CNN	Convolutional neural network
PNN	Probabilistic neural network
SVM	Support vector machine
DDSM	Digital Database for Mammography Screening
Mini-MIAS	Mini Mammographic Image Analysis Society
BraTS	MICCAI brain tumor segmentation
k-NN	k-nearest neighbors
SSIM	Structural index similarity
PSNR	Peak signal-to-noise ratio
QILV	Quality index based on local variance
ELM	Extreme learning machine

The fused features were chosen via the Boltzmann entropy method. Multiple classifiers are given the fused feature vector to compare, which can make predictions with higher accuracy. Tumor estimate was done using the BraTS datasets, which had a mean dice similarity coefficient (DSC) of 0.99. Nazir et al. [12] developed a wavelet transform segmentation method. The high-energy subband of the image was separated into blocks in the first phase of decomposition into wavelet subbands. Discrete cosine transform is used in the second step to choose high-variance features from each block and align them with the neural network for classification and a 99.7% accuracy was attained. Saba et al. [13] proposed the region of interest (ROI) of posttraumatic stress disorder (PTSD) in the brain using resting-state functional magnetic resonance imaging (rs-fMRI), and machine learning algorithms were used to distinguish between PTSD

and healthy controls. For classification, the k-NN and SVM with radial basis function kernel achieved high accuracies of (96.6%, 94.8%, 98.5%) and (93.7%, 95.2%, 99.2%), respectively. The transfer learning AlexNet's convolutional neural network (CNN) utilized by Badjie and Deniz Ülker [14] to classify brain tumor MR images and achieved an accuracy of 99.62% in classifying the tumors. Kurdi et al. [15] proposed Harris hawks optimized convolution network (HHOCNN) with Kaggle dataset and achieved a 98% overall accuracy. Sarmad et al.[16] proposed a specially designed 17-layered deep neural network and used the BraTS 2018 and Figshare datasets and obtained 97.47% accuracy and 98.92% accuracy, respectively. Rajinikanth et al. [17] employed the VGG16 and VGG19 convolutional neural network (CNN) schemes with the SoftMax function and achieved 99% when used with decision tree (DT). Annepu et al. [18] reviewed terrestrial anchor node (FTAN) with soft computing optimization of extreme learning machine (ELM). Annepu et al. [19] uses ELM For node localization in UAV-assisted WSNs. A two-dimensional flexible analytical wavelet transform (FAWT) was proposed by Patel and Kashyap [20] for feature extraction and feature selection by PCA from the SARS-CoV-CT database. The extracted features were fed to least square-SVM (RBF) for classification and achieved an accuracy of 93.47% with tenfold cross-validation. The least square-support vector machine (SVM), Gabor filter bank, and linear discriminant analysis (LDA) were used for classification feature extraction and feature selection for the COVID-19 dataset and achieved a classification accuracy of 93.96% [21]. Further, LS-SVM was used and achieved a classification accuracy of 95.48%, a specificity of 95.37%, a sensitivity of 95.43%, and an $F1$ score of 95 [22]. Patel and Kashyap [23] proposed a novel approach based on bit-plane slicing (BPS), local binary pattern (LBP), and gray-level co-occurrence matrix (GLCM) for LBP images and achieved an accuracy of 95.04%. Singh et al. [24] proposed a novel computer-aided diagnostic network and Gabor-modulated convolutional filter-based classifier for brain tumor classification of brain tumor with BraTS dataset and achieved 98.68% classification accuracy. The ultra-light brain tumor detection (UL-BTD) system was proposed by Qureshi et al. [25] for the diagnosis and surgical resection of brain tumors using magnetic resonance (MR) images. The proposed UL-BTD system introduces a novel ultra-light deep learning architecture (UL-DLA) that incorporates deep features and highly distinctive textural features extracted by the gray-level co-occurrence matrix (GLCM). This combination forms a hybrid feature space (HFS) utilized for tumor detection through support vector machine (SVM) and achieved an average detection rate of 99.23% and an F-measure of 0.99 for glioma, meningioma, and pituitary tumors.

Some of the harmony search-based optimization techniques were applied to different engineering problems. A brand-new binary harmony search (BHS) was put forth by Shi et al. [26] to choose the best channel sets and enhance system accuracy. Enikeeva et al. [27] offered a gravitational search algorithm and the harmony algorithm to address the issues with chemical kinetics, while Bala and Safei [9] proposed a hybrid harmony search and particle swarm optimization algorithm (HSPSO) strategy to speed up algorithm performance. The harmony search algorithm and an artificial neural network for fraud detection were proposed by Daliri [28]. Zhu et al. [29] proposed an autonomous clustering approach (AC-DPHS) based on dynamic parameters of the harmony search optimization technique. K-means clustering was used to estimate the ideal number of clusters automatically using the dynamic parameter harmony search (DPHS). Al-Betar et al. [30] proposed integrating island mode principles into the algorithm's core architecture to enhance the HS algorithm's convergence capabilities. The population's constituents are divided into distinct subpopulations known as islands to enhance performance. Harmony search-based techniques were used by Al-Shamiri et al. [31] to optimize the weights of ELM. The combination of HS algorithms and ELM has produced effective generalization results. Dai et al. [32] proposed a self-adaptive multiobjective harmony search (SAMOHS) algorithm by employing a self-adaptive bandwidth to solve a practical engineering optimization problem. Haghshenas et al. [33] applied a harmony search for slope stability analysis in geotechnical engineering to avoid the risk associated with the occurrence of a landslide. Mansor et al. [34] proposed scheduling and rostering of bus driver problems using a harmony search algorithm. Utilizing the step function, the harmony memory consideration rate (HMCR) parameter is adjusted to optimize the distribution of shifts and routes among drivers. An island-based harmony search technique for economic load dispatch was put forth by Al-Betar [35]. When tracing the contacts of the coronavirus, Al-Shaikh et al. [36] introduced the hybrid harmony search (HHS) approach to locate strongly connected components (SCCs). This method results in a run time increase of 77.18% and a remarkable average error rate of 1.7%. With more computational time, the aforementioned research yields a range of accuracy levels. The sine cosine algorithm (SCA) was proposed in [37, 38] for the optimization problems. Mishra et al. [39] proposed the classification of brain tumors using the modified SCA for local linear radial basis function neural network. The MSCA-APSO was employed to optimize weights and achieved 99% sensitivity, 100% specificity, and 99.61% accuracy. The modified harmony search-sine cosine algorithm (MHS-SCA) that has been proposed is yet to be used for optimization.

3. Materials and Methods

The proposed system architecture is presented in Figure 1. The research flow steps are as follows. (1) The brain tumor images undergo resizing. (ii) The images undergo Mexican hat wavelet transform for feature extraction to make a new feature dataset. (iii) The feature dataset is aligned as input to the proposed MHS-SCA-ELM, SCA-ELM, MHS-ELM, and PSO-ELM.

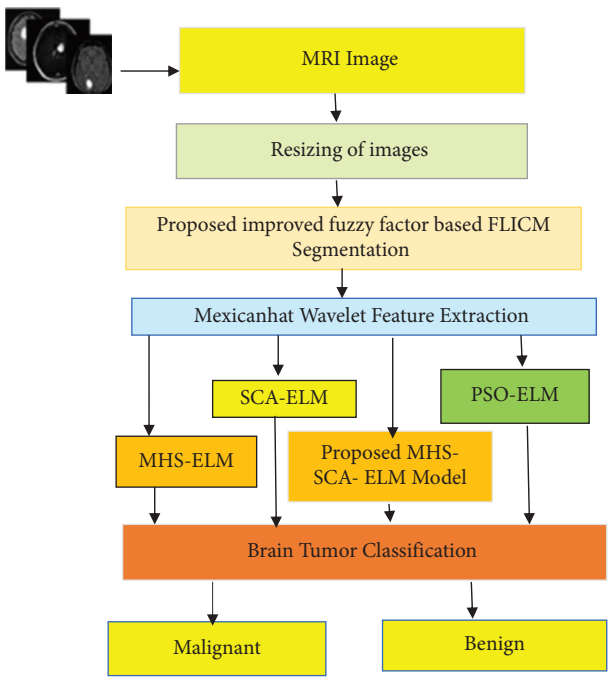

Figure 1: Proposed system architecture.

3.1. Proposed Hybrid MHS-SCA Optimization Algorithm

3.1.1. The Sine Cosine Algorithm (SCA). The sine cosine algorithm (SCA) [37, 38] is a metaheuristic optimization technique that works by simulating the sine and cosine functions, which are periodic, to create a search process that explores the solution space. The SCA begins by randomly generating a population of candidate solutions, which are represented as vectors in the solution space. At each iteration, the algorithm evaluates the fitness of a set of candidate solutions and updates them based on their fitness values and their positions in the solution space. The evaluation is accomplished by the fitness of each candidate solution by an objective function that measures the problem constraints. The best candidate solutions are selected based on their fitness values. The selected solutions are updated by adapting their positions in the solution space based on the sine and cosine functions. The sine and cosine functions played the role of optimization in the search space to reach the destination. The sine and cosine functions are used to update the position of each solution in the search space. The sine and cosine functions converge to zero with a bound limit of [−1, 1]. When the sine and cosine waves tend to move in search space, they achieve new positions at different time intervals.

The updated position equation is given by

$$Z_i^{n+1} = \begin{cases} Z_i^n + \alpha_1 \times \sin(\alpha_2) \times \left|\alpha_3 p^{g\text{best}} - Z_i^n\right|, & \alpha_4 < 0.5, \\ Z_i^n + \alpha_1 \times \cos(\alpha_2) \times \left|\alpha_3 p^{g\text{best}} - Z_i^n\right|, & \alpha_4 \geq 0.5, \end{cases} \tag{1}$$

where α_1, α_2, α_3, and α_4 are the random variables.

The next position in the search is presented by α_1, α_2 determines direction, α_3 controls the current movement, and the parameter α_4 changes constantly among the sine and cosine functions. $p^{g\text{best}}$ is the best position obtained during destination search. α_1 is given by

$$\alpha_1 = a\left(1 - \frac{n}{K}\right), \tag{2}$$

where n and K represent current iteration and maximum iteration, respectively, and a is a constant. The SCA hybridized favorably with modified harmonic search metaheuristic algorithms to improve optimization capability.

3.1.2. Harmony Search Algorithm. The harmony search algorithm is proposed to generate a set of random candidate solutions, called harmonies, and improve them iteratively by adjusting the values of their components, called pitches, to mimic the process of improvising music [40]. In order to attain the best musical note optimization, artists practice, which is the foundation of harmony search (HS) [31, 40, 41]. HS is acknowledged as a metaheuristic optimization algorithm. The artists are thought of as algorithmic decision variables. The same way musicians can improve their sound effects by practicing frequently, optimization objective function results can be improved. The musicians improvise harmony while they are composing using the HS approach. The musicians mix several musical pitches to create a fine tune, which they then memorize for later use. Different HS factors were crucial to optimization, including PAR, HMCR, and PAR. The randomly generated harmony matrix is given by

$$\text{Hsm} = \left[\begin{array}{ccc|c} z_1^1 & \cdots & z_n^1 & f\left(z^1\right) \\ \vdots & \ddots & \vdots & \vdots \\ z_{\text{Hsm}}^1 & \cdots & z_n^{\text{Hs}} & f\left(z^{Hs}\right) \end{array}\right]. \tag{3}$$

Initializing the harmony memory (HM) space containing HMS harmony vectors a probability parameter pitch adjusting rate(PAR) is required as per the "bw" parameter. The BW parameter is the step size tuning parameter. The new harmony vector is defined as

$$z_i^{new} = \begin{cases} z_i^{\text{old}} + \text{rand} \times \text{bw}, & \text{with PAR}, \\ z_i^{\text{old}}, & \text{with } 1 - \text{PAR}, \end{cases} \tag{4}$$

where $\text{bw} = z_i^1 - z_i^2$.

3.1.3. Modified Harmony Search-Sine Cosine Algorithm (MHS-SCA) Optimization Technique. The original HS algorithm's slow convergence rate and tendency to become stuck in local optima were addressed by the modified harmony search (MHS) algorithm, which is an enhanced version of the original HS algorithm.

Now to achieve faster optimization, the harmony vector is modified as

$$\begin{aligned} z_{\mathrm{MHMSi}}^{\mathrm{New}}(n+1) &= z_{\mathrm{MHMSi}}^{\mathrm{Old}}(n) + \left(z_i^1 - z_i^2\right) \times (\mathrm{rand}), \text{with PAR}, \\ z_{\mathrm{MHMSi}}^{\mathrm{New}}(n+1) &= z_{\mathrm{MHMSi}}^{\mathrm{Old}}(n) + \left(z_i^1 - z_i^2\right) \times \chi \times (rand), \text{with } (1-\mathrm{PAR}), \end{aligned} \tag{5}$$

where MHMS is the modified harmony search and χ is the learning parameter.

According to the parameter PAR, a higher PAR probability during the initial iterations aids in adjusting the numerical variables through the pitch stages to enhance the variety of solutions and prevent local optimum.

The PAR is given by

$$\mathrm{PAR} = \exp\left(\frac{\mathrm{It}}{\mathrm{NI}}\right), \tag{6}$$

where It is the maximum iteration and NI is the maximum number of improvisations. We have to choose the PAR parameter to a larger value.

Now combining the sine and cosine algorithm position equation and harmony vector equation, the new position equation is given by

$$z_{\mathrm{MHS-SCA}}^{\mathrm{New}}(n+1) = \begin{cases} z_{\mathrm{MHS-SCA}}^{\mathrm{Old}}(n) + \alpha_1 \sin\left(\left(z_i^1 - z_i^2\right) \times (\alpha_2)\right) \times \left|\alpha_3 p^{g\mathrm{best}} - z_i^n\right| \\ z_{\mathrm{MHS-SCA}}^{\mathrm{Old}}(n) + \alpha_1 \cos\left(\left(z_i^1 - z_i^2\right) \times (\alpha_2)\right) \times \left|\alpha_3 p^{g\mathrm{best}} - z_i^n\right| \end{cases}, \text{with PAR}, \tag{7}$$

$$z_{\mathrm{MHS-SCA}}^{\mathrm{New}}(n+1) = \begin{cases} z_{\mathrm{MHS-SCA}}^{\mathrm{Old}}(n) + \chi \times \alpha_1 \sin\left(\left(z_i^1 - z_i^2\right) \times (\alpha_2)\right) \times \left|\alpha_3 p^{g\mathrm{best}} - z_i^n\right| \\ z_{\mathrm{MHS-SCA}}^{\mathrm{Old}}(n) + \chi \times \alpha_1 \cos\left(\left(z_i^1 - z_i^2\right) \times (\alpha_2)\right) \times \left|\alpha_3 p^{g\mathrm{best}} - z_i^n\right| \end{cases}, \text{with } (1-\mathrm{PAR}). \tag{8}$$

The ELM model's weights will be optimized using the proposed hybrid MHS-SCA technique. The proposed MHS-SCA method selects five benchmark functions for optimization to demonstrate its efficacy. The pseudocode of MHS-SCA optimization is presented in Table 2. The flowchart for MHS-SCA is presented in Figure 2.

For the MHS algorithm, the initialization of parameters and estimates has a complexity of $O(n^2)$. The process model has a complexity of $O(n)$. The number of calculation points used is $2n+1$, so the computational complexity of the SCA per time step is $O(n^3)$. For the MHS-SCA, computation for the entire calculation is measured as $O(n \log_2 n^2)$.

3.2. Proposed MHS-SCA-Based Extreme Learning Machine

3.2.1. ELM Model. The ELM algorithm is a machine learning model consisting of a single hidden layer and randomly generated connection weights between the input and hidden layers. The ELM model [42] is a feed-forward neural network in which the output layer weights are computed analytically to make the convergence process fast and efficient. The weights of the extreme learning machine (ELM) [43, 44] are tuned with the MHS algorithm in accordance with the robustness and quicker convergence performance of the improved harmony search method. ELM is a reliable network that performs well in terms of generalization. It is suggested that the current ELM model combined with MHS learning be used to achieve better generalization outcomes. The model architecture is proposed in Figure 3.

The output function of ELM [43] with N hidden neurons is represented:

$$y = \sum_{n=0}^{N} \beta_n f_n(w_n; x), \tag{9}$$

where $f(w; x) = [1, f_1(w_1; x), \ldots\ldots, f_n(w_n; x)]$ is the hidden weight and β is the weight which can be expressed as

$$F\beta = y, \tag{10}$$

where F is "feature-mapping matrix" given by

$$F = \begin{bmatrix} 1 & F_1(w_1; x_1) & \cdots & F_L(w_n; x_1) \\ \vdots & \vdots & \vdots & \vdots \\ 1 & F_1(w_1; x_N) & \cdots & F_L(w_n; x_N) \end{bmatrix}, \tag{11}$$

And $\hat{\beta} = F^{\dagger} d$.

Then, equation (7) can be written as

$$F^{\dagger} = \left(F^T F\right)^{-1} F^T, \tag{12}$$

where $F^{\dagger}$ is the "Moore–Penrose generalized inverse of matrix" and d is the desired vector.

The desired vector is given by $d = \begin{bmatrix} d_1 \\ d_2 \\ \vdots \\ d_n \end{bmatrix}$, and $\hat{\beta} = \begin{bmatrix} \beta_1 \\ \beta_1 \\ \vdots \\ \beta_n \end{bmatrix}$.

According to the extreme learning machine, the output layer is defined with weights as

Table 2: Pseudocode: MHS-SCA optimization algorithm implementation.

Pseudocode: MHS-SCA optimization algorithm

(1) Initialize harmony search parameters PAR, It, NI, χ
(2) Initialize the SCA parameters $\alpha_1, \alpha_2, \alpha_3, \alpha_4$
(3) Calculate the harmony vector based on z_i^{new}
(4) Fitness function evaluation based on $z_{\text{MHS-SCA}}^{\text{New}}$
(5) % Loop for optimization
(6) For $i = 1 : n$
(7) Update SCA parameter to obtain fitness using equation (1)
(8) Update the HS parameter PAR = exp (It/NI)
(9) Update the modified position equation

$$(10)\ z_{\text{MHS-SCA}}^{\text{New}}(n+1) = \begin{cases} z_{\text{MHS-SCA}}^{\text{Old}}(n) + \alpha_1 \sin((z_i^1 - z_i^2) \times (\alpha_2)) \times |\alpha_3 p^{g\text{best}} - z_i^n| \\ z_{\text{MHS-SCA}}^{\text{Old}}(n) + \alpha_1 \cos((z_i^1 - z_i^2) \times (\alpha_2)) \times |\alpha_3 p^{g\text{best}} - z_i^n| \end{cases}, \text{ with PAR}$$

$$(11)\ z_{\text{MHS-SCA}}^{\text{New}}(n+1) = \begin{cases} z_{\text{MHS-SCA}}^{\text{Old}}(n) + \chi \times \alpha_1 \sin((z_i^1 - z_i^2) \times (\alpha_2)) \times |\alpha_3 p^{g\text{best}} - z_i^n| \\ z_{\text{MHS-SCA}}^{\text{Old}}(n) + \chi \times \alpha_1 \cos((z_i^1 - z_i^2) \times (\alpha_2)) \times |\alpha_3 p^{g\text{best}} - z_i^n| \end{cases} \text{ with (1-PAR)}$$

(12) Choose the maximum optimized $z_{\text{MHS-SCA}}^{\text{New}}$ values between equations (7) and (8)
(13) end for the loop i
(14) Stopping criteria: Converge up to optimal solution, else go to step 6

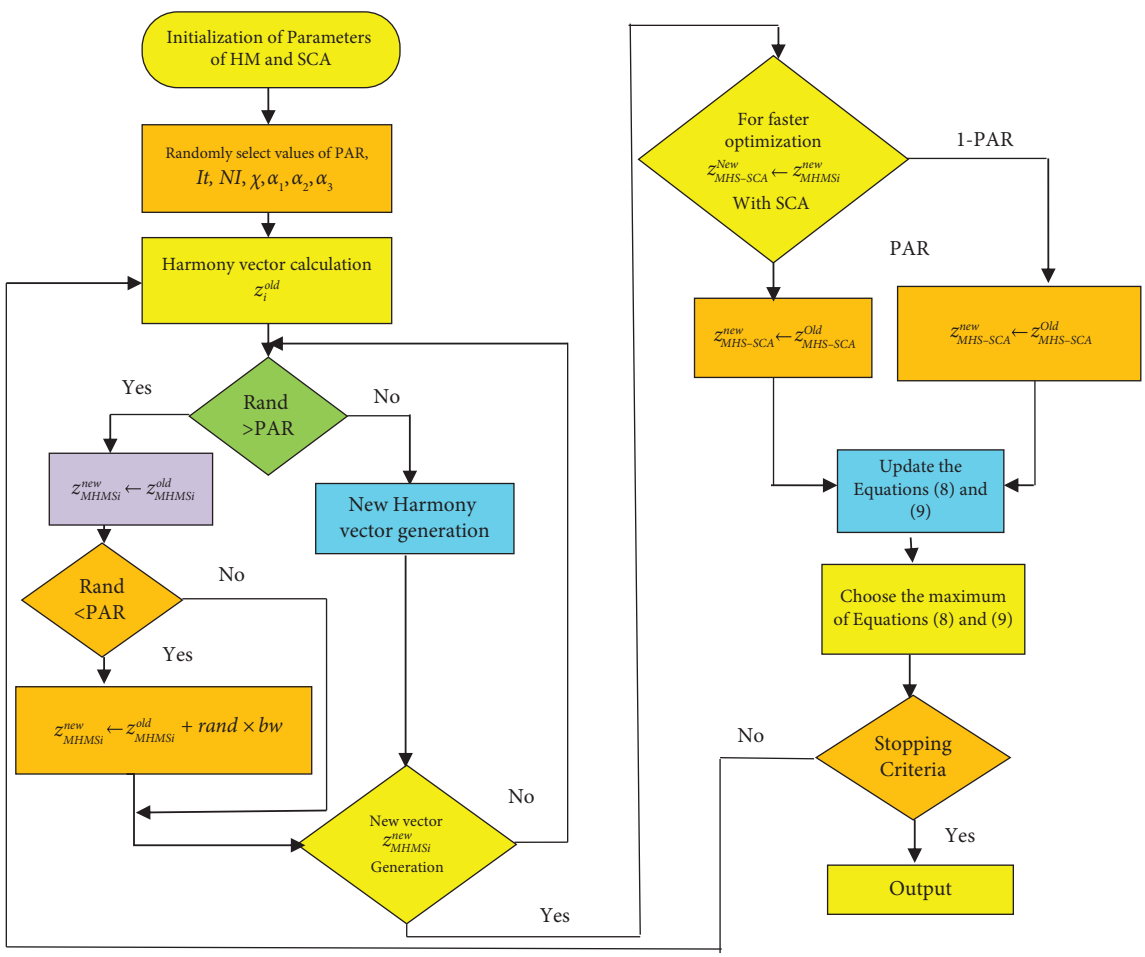

Figure 2: Flowchart of MHS-SCA.

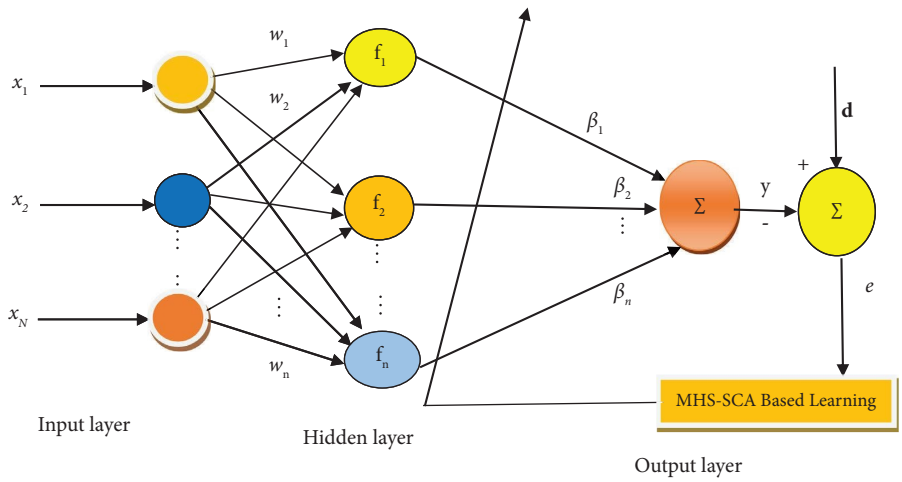

Figure 3: MHS-SCA-based ELM model.

$$\widehat{\beta} = \left(F^T F\right)^{-1} F^T \begin{bmatrix} d_1 \\ d_2 \\ \vdots \\ d_n \end{bmatrix}. \tag{13}$$

Now, the weights of the matrix will be optimized by the MHS-SCA to improve the performance of the ELM model.

3.2.2. Weight Optimization by MHS-SCA. To achieve the optimization, the weights $W = [w_1, w_2 \ldots\ldots\ldots w_n]$ are maintained in the "harmony memory (HM) matrix," and the matrix is taken into account with the "harmony memory size (HMS)," and the weight matrix is generated randomly. W_{MHMS} is the weight matrix, where the subscript MHMS represents the abbreviation as "modified harmonic search."

Now considering the new learning parameter χ for faster convergence with "PAR (pitch adjusting rate; $0 \le \text{PAR} \le 1$)," the new weight is given by

$$w_{\text{MHMSi}}^{\text{New-PAR}}(n+1) = w_{\text{MHMSi}}^{\text{Old}}(n) + \text{bw} \times (\text{rand} - 1), \text{ with PAR}, \tag{14}$$

where "bw" is the "maximum change in pitch adjustment."

The new weight updated equation is given by

$$w_{\text{MHMSi}}^{\text{New}}(n+1) = w_{\text{MHMSi}}^{\text{Old}}(n) + \text{bw} \times \chi \times (\text{rand}), \text{ with } 1 - \text{PAR}. \tag{15}$$

Now considering the weight vectors combining with the sine and cosine algorithm position equation and harmony vector equation, the updated position equation is given by

$$\begin{aligned} w_{\text{MHS-SCA}}^{\text{New-PAR}}(n+1) &= \begin{cases} w_{\text{MHS-SCA}}^{\text{Old}}(n) + \alpha_1 \sin\left(\left(z_i^1 - z_i^2\right) \times (\alpha_2)\right) \times \left|\alpha_3 p^{g\text{best}} - z_i^n\right| \\ w_{\text{MHS-SCA}}^{\text{Old}}(n) + \alpha_1 \cos\left(\left(z_i^1 - z_i^2\right) \times (\alpha_2)\right) \times \left|\alpha_3 p^{g\text{best}} - z_i^n\right| \end{cases}, \text{with PAR}, \\ w_{\text{MHS-SCA}}^{\text{New}}(n+1) &= \begin{cases} w_{\text{MHS-SCA}}^{\text{Old}}(n) + \chi \times \alpha_1 \sin\left(\left(z_i^1 - z_i^2\right) \times (\alpha_2)\right) \times \left|\alpha_3 p^{g\text{best}} - z_i^n\right| \\ w_{\text{MHS-SCA}}^{\text{Old}}(n) + \chi \times \alpha_1 \cos\left(\left(z_i^1 - z_i^2\right) \times (\alpha_2)\right) \times \left|\alpha_3 p^{g\text{best}} - z_i^n\right| \end{cases}, \text{with } (1 - \text{PAR}), \end{aligned} \tag{16}$$

where χ is the new learning parameter for optimization. When the values of the weight vector $w_{\text{MHS-SCA}}^{\text{Old}} > w_{\text{MHS-SCA}}^{\text{New-PAR}}$, choose the new weight vector value as $W = w_{\text{MHS-SCA}}^{\text{New}}$. If $w_{\text{MHS-SCA}}^{\text{New-PAR}} > w_{\text{MHS-SCA}}^{\text{New}}$, choose the weight vector value as $W_{PAR} = w_{\text{MHS-SCA}}^{\text{New-PAR}}$. Then select the maximum of weight vectors of both as $\max_w([W_{\text{PAR}}\, W])$.

Now considering the maximum values of the weights, the new Moore–Penrose generalized inverse of matrix is given by

$$F^{\dagger}_{\text{MHS-SCA}} = \left(F^{T}_{\text{MHS-SCA}} F_{\text{MHS-SCA}}\right)^{-1} F^{T}_{\text{MHS-SCA}}, \tag{17}$$

where

$$F_{\text{MHS-SCA}} = \begin{bmatrix} 1 & F_1\left(w^{\text{New}}_{1\text{MHS-SCA}}; x_1\right) & \cdots & F_L\left(w^{\text{New}}_{\text{NMHS-SCA}}; x_1\right) \\ \vdots & \vdots & \vdots & \vdots \\ 1 & F_1\left(w^{\text{New}}_{1\text{MHS-SCA}}; x_N\right) & \cdots & F_L\left(w^{\text{New}}_{\text{NMHS-SCA}}; x_N\right) \end{bmatrix}, \tag{18}$$

$$\text{Then } \hat{\beta} = F_{\text{MHS-SCA}}{}^{\dagger} d.$$

The mean square error is written as

$$E = \frac{1}{n}\sum_{k=1}^{n}\left(d - y_k\right)^2 = \frac{1}{n}\sum_{k=1}^{n}\left[e_k^2\right]. \tag{19}$$

By considering the 1000 iterations for the convergence, the mean square error is calculated by utilizing equation (19) and presented in Section 4. Table 3 displays the MHS-SCA's pseudocode for weight optimization of the ELM model. The framework for brain tumor segmentation and classification is shown in Figure 4.

3.3. Proposed Improved Fuzzy Factor-Based FLICM Segmentation. To improve the effectiveness of FCM-based segmentation algorithms for the detection of brain cancers, an improved fuzzy factor-based fuzzy local information C means (IFF-FLICM) segmentation is presented. The proposed IFF-FLICM segmentation approach enhances the accuracy and reliability of tumor segmentation by incorporating a fuzzy factor in the clustering process to handle uncertainties in medical imaging. Additionally, the local information of each pixel is considered to improve the clustering performance, resulting in a more precise tumor segmentation. FCM segmentation techniques are generally used for noise reduction and detecting tumors from MRI images.

Enhanced fuzzy C means (EnFCM) [2] method claims the objective function as

$$J_s = \sum_{v=1}^{N}\sum_{k=1}^{c} u_{kv}^{m}\left\|x_v - v_k\right\|^2. \tag{20}$$

To improve the noise reduction capability, the fuzzy factor is introduced in the objective function of EnFCM. The fuzzy factor was proposed by Krinidis and Chatzis [45] and was named as fuzzy local information fuzzy C means (FLICM). The objective function with fuzzy factor is given by

$$J_{\text{FLICM}} = \sum_{l=1}^{N}\sum_{k=1}^{c} u_{kl}^{m}\left\|x_l - v_k\right\|^2 + + \sum_{l=1}^{N}\sum_{k=1}^{c} \text{Q}_{\text{kl}}, \tag{21}$$

where N is the total number of pixels in image, C denotes the cluster centre, and "m" determines the fuzziness of the consequential partition. u_{kl} is the fuzzy partition matrix. The fuzzy factor is given by

$$\text{Q}_{\text{kl}} = \sum_{\substack{r\in N_l \\ l\neq r}} \frac{1}{d_{lr}+1}\left(1 - u_{\text{kl}}\right)^m \left\|x_l - v_k\right\|^2, \tag{22}$$

where d_{lr} is the Euclidean distance between the pixels.

The fuzzy factor is boosted to enhance the FLICM segmentation's capacity to reduce noise, and the enhanced fuzzy factor is provided by

$$\text{Q}_{\text{kl}}^{\text{iff}} = \sum_{\substack{r\in N_l \\ l\neq r}} \frac{1}{d_{lr}+1}\log\left(\left(1 - u_{kl}\right)^m \left\|x_l^{\gamma+1} - v_k\right\|^2\right), \tag{23}$$

where γ is the smoothness parameter of the pixels and the values are defined in between [0, 1].

$$u_{kl} = \frac{1}{\sum_{p=1}^{c}\left(\left\|x_l - v_k\right\|^2 + \text{Q}_{\text{kl}}\,\%/\left\|x_l - v_p\right\|^2 + \text{Q}_{\text{pv}}\right)^{1/m-1}}, \tag{24}$$

and

$$v_k = \frac{\sum_{k=1}^{N} u_{kl}^{m} x_l}{\sum_{l=1}^{N} u_{\text{kl}}}. \tag{25}$$

The new objective function of improved fuzzy factor FLICM is given by

$$J_{\text{FLICM}}^{\text{iff}} = \sum_{l=1}^{N}\sum_{k=1}^{c} u_{kl}^{m}\left\|x_l - v_k\right\|^2 + \sum_{l=1}^{N}\sum_{k=1}^{c} \text{Q}_{\text{kl}}^{\text{iff}}, \tag{26}$$

where the superscript iff indicates the improved fuzzy factor. The median filter is appled to the fuzzy partiton matrix to improve the segmentation capability. The new

Table 3: Pseudocode: MHS-SCA for weight optimization of the ELM model.

Pseudocode
(1) **Input**: Initializing particles (ELM weights) $W = [w_1, w_2 \ldots\ldots\ldots w_n]$ randomly
(2) **Input**: Initialize the MHS parameters μ, bw, rand, χ
(3) **Output**: Calculation of error
(4) %Program loop
(5) For $i = 1 : n$
(6) "%" Weight updation with PAR
(7) $w_{\text{MHS-SCA}}^{\text{New-PAR}}(n+1) = \begin{cases} w_{\text{MHS-SCA}}^{\text{Old}}(n) + \alpha_1 \sin((z_i^1 - z_i^2) \times (\alpha_2)) \times \lvert \alpha_3 p^{g\text{best}} - z_i^n \rvert \\ w_{\text{MHS-SCA}}^{\text{Old}}(n) + \alpha_1 \cos((z_i^1 - z_i^2) \times (\alpha_2)) \times \lvert \alpha_3 p^{g\text{best}} - z_i^n \rvert \end{cases}$
(8) % Obtain new optimization with 1-PAR
(9) $w_{\text{MHS-SCA}}^{\text{New}}(n+1) = \begin{cases} w_{\text{MHS-SCA}}^{\text{Old}}(n) + \chi \times \alpha_1 \sin((z_i^1 - z_i^2) \times (\alpha_2)) \times \lvert \alpha_3 p^{g\text{best}} - z_i^n \rvert \\ w_{\text{MHS-SCA}}^{\text{Old}}(n) + \chi \times \alpha_1 \cos((z_i^1 - z_i^2) \times (\alpha_2)) \times \lvert \alpha_3 p^{g\text{best}} - z_i^n \rvert \end{cases}$
(10) If $w_{\text{MHS-SCA}}^{\text{New}} > w_{\text{MHS-SCA}}^{\text{New-PAR}}$
(11) Choose the weight vector value as $W = w_{\text{MHS-SCA}}^{\text{New}}$
(12) end
(13) If $w_{\text{MHS-SCA}}^{\text{New-PAR}} > w_{\text{MHS-SCA}}^{\text{New}}$
(14) Choose the weight vector value as $W_{\text{PAR}} = w_{\text{MHS-SCA}}^{\text{New-PAR}}$
(15) end
(16) Select the maximum weights of both as $\max_w([W_{\text{PAR}}\, W])$
(17) Choose the best weight until the convergence criterion is satisfied % calculate mean square error
(18) $E(i) = 1/n \sum_{i=1}^{n} [e_i^2]$
(19) End for the loop i
(20) Continue the procedure till convergence is satisfied, else repeat step 4 to step 19

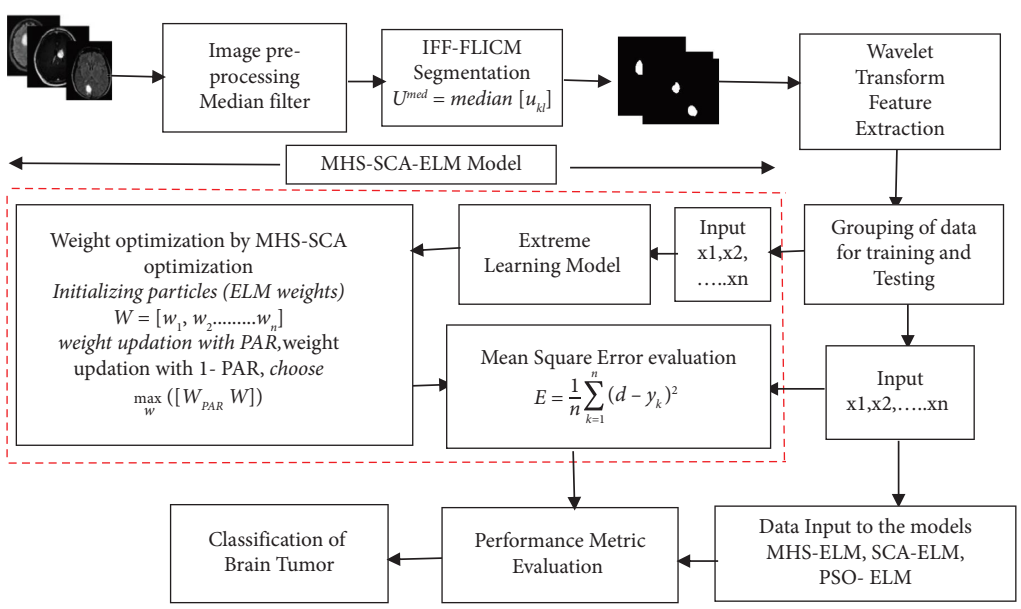

Figure 4: Proposed framework for segmentation and classification of brain tumor.

fuzzy partition matrix is given by $U^{\text{med}} = \text{median}[u_{\text{kl}}]$. The parameters used for the simulation are presented in Table 4.

3.4. Database. The Medical School of Harvard University generated Dataset-255, which contains "255 (35 normal and 220 pathological) 256×256 axial plane brain scans" [39].

Table 4: Parameters for simulation.

Algorithms	Parameters	Value
Harmony search	Iterations	1000
	bw	0.6
	χ	0.8
	rand	[0, 1]
SCA	$\alpha_1, \alpha_2, \alpha_3$	[0, 1]
FLICM	m	2
	γ	[0, 1]

Dataset-255 contains aberrant brain MR scans from 11 different disorders, including Alzheimer's disease. Four novel illnesses, including chronic subdural hematoma, cerebral toxoplasmosis, herpes encephalitis, and multiple sclerosis, are represented by aberrant images in Dataset-255. Out of 255 images, 204 images were taken for training and 51 images for testing. The 204 images, 80% out of 255 images, containing 176 abnormal and 28 normal images, are presented in Table 5.

3.5. Mexican Hat Wavelet Transform and Feature Extraction. Discrete wavelet transform [30] with Mexican hat wavelet has been utilized to extract features from the segmented images. The Mexican hat wavelet function is given by

$$\psi(x) = \frac{2}{\sqrt{3\sigma}\pi^{1/4}}\left(1 - \left(\frac{x}{\sigma}\right)^2\right)e^{-x^2/2\sigma^2}, \tag{27}$$

where σ is the standard deviation controlling the smoothness and ψ is the wavelet function.

The images are applied to the median filter for preprocessing at the first instance. The images are filtered by utilizing the median filter to enhance the image quality by removing the noise. The wavelet transform acts as filter and is also applied for feature extraction purpose. A total 204 of images are considered for training, which is 80% of the total 255 images. 51 images are taken for testing, which is 20% of the images. The seven features such as "power spectral density (PSD)," "Kurtosis," and "Shannon entropy, energy, mean, dispersion entropy, and standard deviation" [39] are extracted from the images and grouped for training and testing dataset. A total of 1785 features are extracted by utilizing seven features ($255 \times 7 = 1785$) and utilized as training and testing dataset for classification purposes. Training and testing data are separated in the database. The training data is taken as 80% which is calculated as ($204 \times 7 = 1628$) and the testing data taken as 20%, which is calculated as ($51 \times 7 = 357$) data from the total dataset. The training dataset and testing dataset are aligned to PSO-ELM, SCA-ELM, and MHS-ELM and proposed MHS-SCA-ELM for classifying the data into cancerous and noncancerous categories. The training and testing results are presented in Table 6.

3.6. Validation of Modified Harmony Search-Sine Cosine Algorithm (MHS-SCA). The proposed modified harmony search algorithm is tested with the five benchmark functions ($F1$–$F5$) [39] presented in Table 7. Out of five benchmark functions, four multimodal functions and one unimodal function are used for optimization. To show the dominance of the proposed MHS-SCA optimization algorithm, other metaheuristic optimization algorithms PSO [39], MHS, and SCA [38] are considered.

Particle swarm optimization (PSO) techniques are based on bird flocking. The PSO, HS, and SCA are the optimization techniques utilized for the weight optimization of several machine learning models. The models such as PNN [40], SVM [31], "local linear radial basis function neural network (LLRBFNN)" [41], feed-forward neural network [37], ELM [44], and CNN [46, 47] were proposed for brain tumor classifications from MRI images with different metaheuristic optimization techniques. The MHS-SCA is the new algorithm proposed for weight optimization of the ELM model in our research. The "sine cosine algorithm (SCA)" [38] is created on sine and cosine function position change due to the involvement of the random movement directions in the search space. All five functions are optimized by employing PSO [39], SCA [38], MHS, and proposed MHS-SCA optimization algorithms.

3.7. Segmentation Performance Measures. Peak signal-to-noise ratio (PSNR) [48] is a simpler and more traditional metric based solely on pixel-wise error; SSIM provides a more comprehensive assessment by considering structural information and mimicking aspects of human visual perception. PSNR is calculated based on the mean squared error between the original image and the distorted image. The formula is often expressed as

$$\mathrm{PSNR} = 10 \cdot \log_{10}\left(\frac{\mathrm{Max}^2}{\mathrm{MSE}}\right), \tag{28}$$

where Max is the maximum possible pixel value and MSE is the mean squared error. PSNR measures the ratio of the maximum possible power of a signal to the power of corrupting noise that affects the quality of its representation. Higher PSNR values indicate better image quality.

Structural similarity index (SSIM) [48] assesses the structural information and similarity between the reference and distorted images. SSIM considers aspects such as texture and structural information in addition to pixel values.

$$\mathrm{SSIM}(x, y) = \frac{\left(2\mu_x\mu_y + C_1\right)\left(2\sigma_{xy} + C_2\right)}{\left(\mu_x^2 + \mu_y^2 + C_1\right)\left(\sigma_x^2 + \sigma_y^2 + C_2\right)}, \tag{29}$$

Table 5: Details of Dataset-255.

Dataset	Total number of images		Training images		Testing images	
	Normal	Abnormal	Normal	Abnormal	Normal	Abnormal
Dataset-255	35	220	28	176	7	44

Table 6: Classifiers' performance evaluation.

Model	No. of iterations	Training accuracy (%)	Testing accuracy (%)	Sensitivity (%)	Specificity (%)	Computational time (sec)
PSO-ELM	1000	93.12	91.58	91.65	88.58	79.6528
MHS-ELM	1000	95.23	93.28	94.13	91.78	58.3321
SCA-ELM	1000	97.33	96.54	97.45	98.65	32.2657
MHS-SCA-ELM	1000	**99.12**	**98.47**	**98.78**	**99.23**	**23.2487**

Table 7: Benchmark functions for optimization of the proposed MHS-SCA.

Function	Name of the function	Details	Dimension	Bound regions
$F1$ [39]	Multimodal	"$\sum_{i=1}^{n}[x_i^2 - 10\cos(2\pi x_i) + 10]$"	20	[−5.12, 5.12]
$F2$ [39]	Multimodal	$-20\exp\left(-0.2\sqrt{1/n\sum_{i=1}^{n}x_i^2}\right) - \exp\left(1/n\sum_{i=1}^{n}\cos(2\pi x_i)\right) + 20 + e$	20	[−32, 32]
$F3$ [39]	Multimodal	$1/4000\sum_{i=1}^{n}x_i^2 - \prod_{i=1}^{n}\cos(\frac{x_i}{\sqrt{i}}) + 1$	20	[−600, 600]
$F4$ [39]	Multimodal	$\sum_{i=1}^{n} - x_i\sin(\sqrt{\lvert x_i\rvert})$	20	[−500, 500]
$F5$ [39]	Unimodal	$\sum_{i=1}^{n}\lvert x_i\rvert + \prod_{i=1}^{n}\lvert x_i\rvert$	20	[−10, 10]

where μ_x and μ_y are the mean intensities of x and y, σ_x^2 and σ_y^2 are the variances, σ_{xy} is the covariance, and C_1 and C_2 are the constants to stabilize the division with weak denominator.

3.8. Classification Performance Measure. MHS-ELM, SCA-ELM, PSO-ELM, and the proposed MHS-SCA based ELM model achieve the classification of the brain tumor. The classifiers' performances are obtained by computing accuracy, computational time, specificity, and sensitivity. For this experiment, 1000 iterations were considered, and the results of each category are presented in Table 6.

$$\text{Sensitivity} = \text{TPR} = \frac{\text{TP}}{\text{TP} + \text{FN}},$$
$$\text{Specificity} = \text{TNR} = \frac{\text{TN}}{\text{TN} + \text{FP}}, \quad (30)$$
$$\text{Accuracy} = \frac{\text{TP} + \text{TN}}{\text{TP} + \text{TN} + \text{FP} + \text{FN}}.$$

4. Results

4.1. Modified Harmony Search Algorithm Validation Result. Five benchmark functions are optimized by SCA, MHS, PSO, and the proposed MHS-SCA optimization algorithm, and results are presented in Figures 5–9.

The validation of function $F1$ using the SCA, MHS, PSO, and proposed MHS-SCA is shown in Figure 5. The proposed MHS-SCA method converges more quickly than the mentioned PSO, SCA, and MHS algorithms. The proposed MHS-SCA needed around 50 iterations to reach convergence. In contrast, SCA, MHS, and PSO required about 100, 190, and 220 iterations, respectively, as can be seen in Figure 5. The subfigure shows the clarity about the convergence curves of each algorithm. To differentiate the iterations required for MHS and PSO, the subfigure is mentioned and marked with an arrow mark. The iterations required for the convergence of MHS and PSO are clearly shown. The lines in green and black also show the MHS-SCA and SCA convergence curves. Additionally, the PSO, MHS, and SCA achieved ideal values of 0.75759, 0.43609, and 0.29418 for function $F1$, but the proposed MHS acquired an optimal value of 0.18868. One thousand simulation iterations are used for all benchmark function optimizations. The best parameters and iterations for convergence demonstrate the proposed MHS-SCA's robustness. Table 7 shows the optimal values obtained by the different algorithms.

Figure 6 presents the validation of function $F2$. Figure 4 shows that the proposed MHS took nearly 100 iterations, whereas SCA, MHS, and PSO took nearly 200, 210, and 320 iterations for convergence. To differentiate the convergence lines, the subfigure is mentioned in Figure 6. From the subfigure, we can easily identify the iteration required for MHS-SCA; other curves can be seen from the main figure.

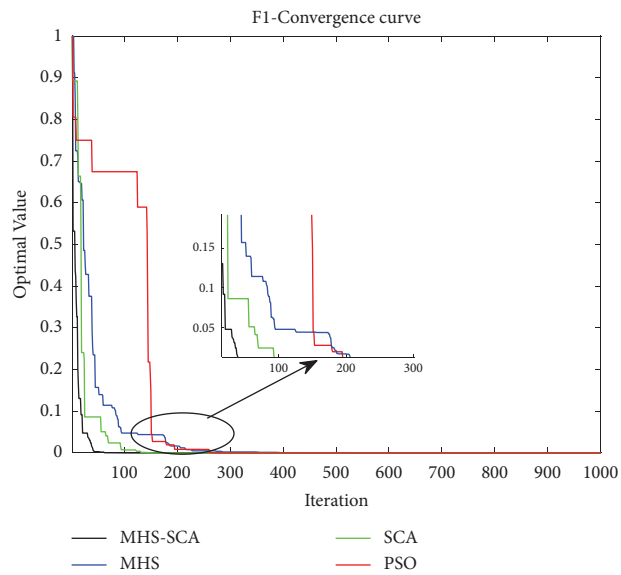

Figure 5: Validation of function $F1$ using PSO, MHS, SCA, and MHS-SCA.

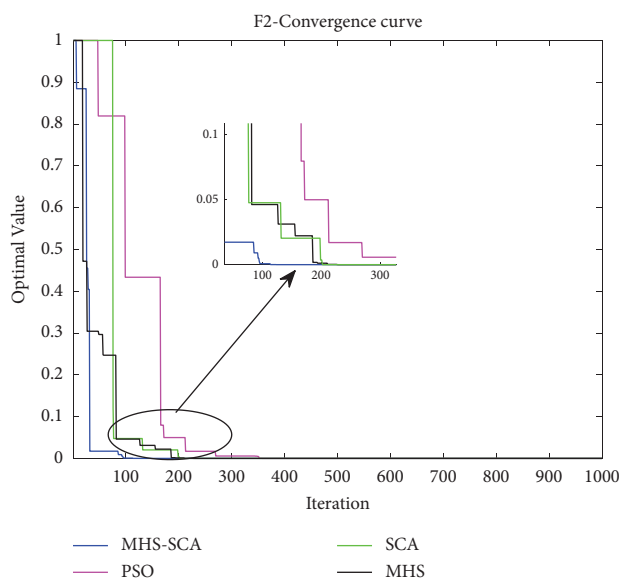

Figure 6: Validation of function $F2$ using PSO, MHS, SCA, and MHS-SCA.

The proposed MHS-SCA achieved an optimal value of 0.18353 for function $F2$, whereas PSO, MHS, and SCA achieved optimal values of 0.71184, 41268, and 0.26211.

The validation of function $F3$ is shown in Figure 7. According to Figure 7, the suggested MHS-SCA required only around 250 iterations, whereas SCA, MHS, and PSO required about 300, 310, and 350 iterations, respectively, to reach convergence. The convergence iterations are discovered to be distinct from the primary. The iteration that SCA, MHS, and PSO took is clearly depicted in the subfigure of Figure 7. Additionally, the PSO, MHS, and SCA achieved ideal values of 0.66278, 0.38888, and 0.19526 for function $F3$, while the proposed MHS acquired an optimal value of 0.17603 for that function.

Figure 8 presents the validation of function $F4$. Figure 8 shows that the proposed MHS-SCA took 190 iterations, whereas SCA, MHS, and PSO took nearly 250, 290, and 450 iterations for convergence. The subfigure clarifies the iteration needed for MHS-SCA and is marked with an arrow mark. An optimal value of 0.17423 is obtained by the proposed MHS-SCA for function $F4$, whereas PSO, MHS, and SCA achieved optimal values of 0.66504, 32961, and 0.26617.

Figure 9 shows that the proposed MHS-SCA took nearly 50 iterations, whereas SCA, MHS, and PSO took nearly 130, 220, and 250 iterations for convergence. The convergence curves are not clearly shown in Figure 9. The subfigure clearly shows the iteration needed for the SCA and MHS

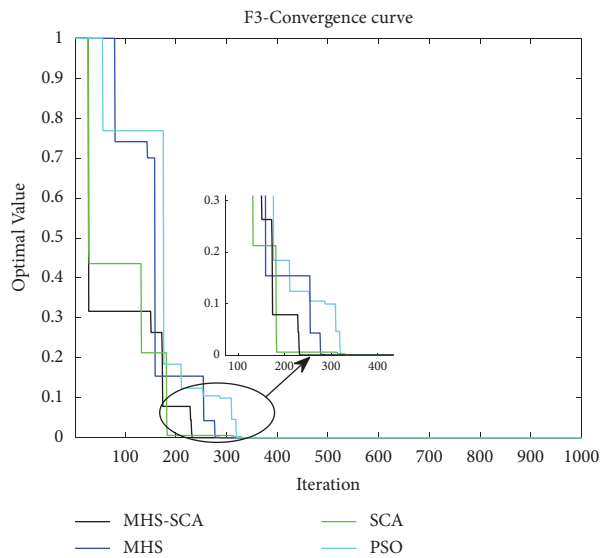

Figure 7: Validation of function $F3$ using PSO, MHS, SCA, and MHS-SCA.

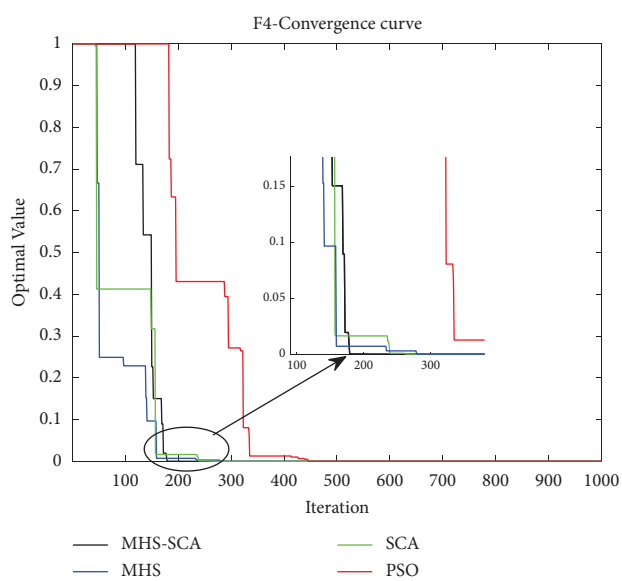

Figure 8: Validation of function $F4$ using PSO, MHS, SCA, and MHS-SCA.

algorithms. Further, the proposed MHS-SCA achieved an optimal value of 0.16249 for function $F5$, whereas PSO, MHS, and SCA achieved optimal values of 0.69023, 32825, and 0.29454. The optimal values are presented in Table 8.

Table 8 shows the optimum values for PSO, MHS, SCA, and MHS-SCA. All the benchmark functions $F1$–$F5$ achieved good optimal values in the proposed MHS-SCA, showing superiority compared to PSO, MHS, and SCA optimization algorithms. The comparison bar result is presented in Figure 10.

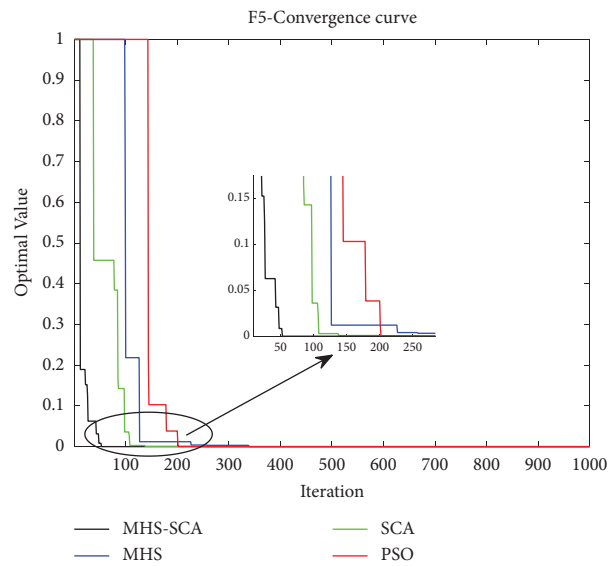

Figure 9: Validation of function $F5$ using PSO, MHS, SCA, and MHS-SCA.

4.2. Brain Tumor Segmentation Results. EnFCM, NDFCM, FLICM, and proposed IFF-FLICM segmentation techniques accomplished the brain tumor segmentation. The Rician noise was reduced, and tumor detection using the proposed IFF-FLICM segmentation technique obtained 99.37% accuracy.

The EnFCM segmentation was employed for the brain tumor image with noise. The noise removal capability of the EnFCM segmentation technique is improper due to the biased character of the controlling parameter. The detection tumor is not obtained correctly, which can be seen from Figure 11. The SSIM value obtained is 0.7324, and PSNR is 23.17, and the lower values of PSNR and SSIM indicate the poor detection capability of the EnFCM algorithm.

The NDFCM segmentation automatically tunes the trade-off parameter by calculating the local variance of gray levels to improve the detection capability. It can be observed from Figure 12 that, still, the detection needs to be up to the required levels because NDFCM uses more parameters during segmentation. The SSIM and PSNR values were obtained as 0.8954, and 28.54 db, which are higher than those of the EnFCM segmentation, but the still values of SSIM and PSNR are less.

The FLICM segmentation replaced the controlling parameter with the fuzzy factor and obtained the SSIM and PSNR values as 0.9317 and 32.59 db. SSIM and PSNR are higher than those of the EnFCM and NDFCM presented in Figure 13, which shows better segmentation capability. Also, a segmentation accuracy of 98.92% was obtained, which is also higher than that of the EnFCM and NDFCM segmentation techniques, which can be observed in Table 9.

Table 8: Optimal values of benchmark functions.

Algorithms	No. of iterations	Optimal values of objective function				
		$F1$	$F2$	$F3$	$F4$	$F5$
PSO	1000	0.75759	0.71184	0.66278	0.66504	0.69023
MHS	1000	0.43609	0.41268	0.38888	0.32961	0.32825
SCA	1000	0.29418	0.26211	0.19526	0.26617	0.29454
MHS-SCA	1000	**0.18868**	**0.18353**	**0.17603**	**0.17423**	**0.16249**

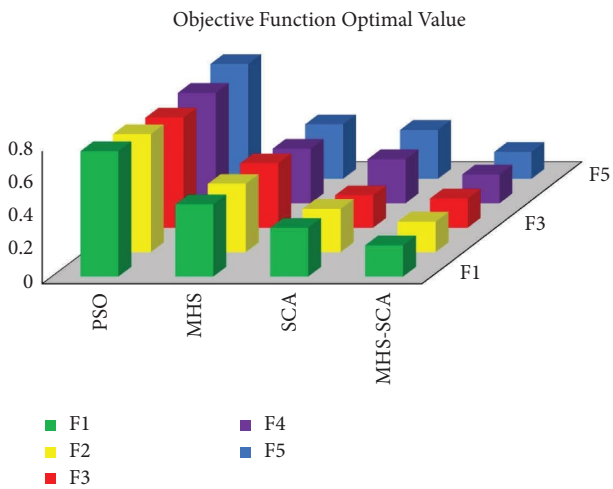

Figure 10: Comparison of optimal values for functions $F1$–$F5$ using PSO, HS, SCA, and MHS algorithms.

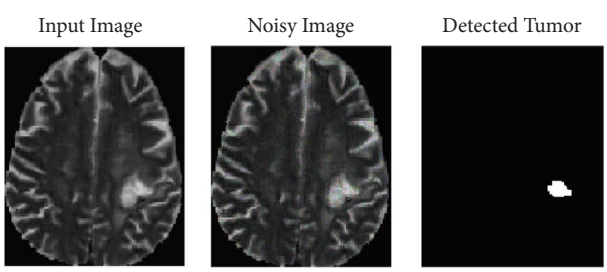

Figure 11: Segmentation of brain tumor using EnFCM.

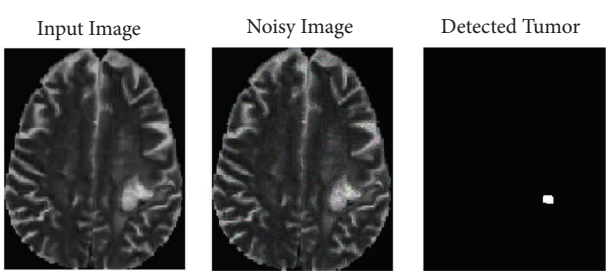

Figure 12: Segmentation of brain tumor using NDFCM.

Further, to improve the segmentation performance of the FLICM, the fuzzy factor is improved in the fuzzy partition matrix and passed through the median filter. It can be observed from Figure 14 that the segmentation IFF-FLICM technique outperformed the other FCM-based segmentation techniques. The SSIM and PSNR achieved 0.9823 and 37.24, higher values than the EnFCM, NDFCM, and FLICM segmentation techniques.

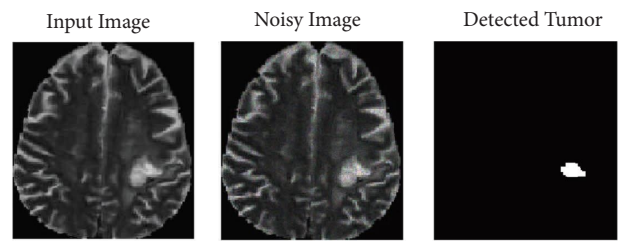

Figure 13: Segmentation of brain tumor using FLICM.

Table 9: Comparison of segmentation accuracy.

Algorithm	Rician noise level $\sigma_n = 10$
EnFCM	96.29
NDFCM	97.84
FLICM	98.92
IFF-FLICM	99.37

The brain tumor segmentation using techniques such as EnFCM, NDFCM, FLICM, and proposed IFF-FLICM is presented in Figures 11–14. The Rician noise is involved in the MRI images during the acquisition of images from the patients. Figure 11 shows the segmentation of brain tumor using the EnFCM technique. The segmentation accuracy was calculated when the Rician noise of $\sigma_n = 10$ was present in the image. It is observed from Figure 11 that the noise reduction is less and the detected tumor was not accurate. The segmentation accuracy obtained by the EnFCM is 96.19%. Figure 12 shows NDFCM segmentation which achieved an accuracy of 97.84%, and the tumor was not properly obtained due to the involvement of the noise. Figure 13 shows the somehow better noise reduction capability by utilizing the FLICM segmentation. The FLICM segmentation provides an accuracy of 98.92%. The location of the tumor is nearly appropriate with an accuracy of 99.37% by utilizing the proposed IFF-FLICM segmentation. The brain tumor segmentation of the IFF-FLICM is shown in Figure 14. The segmentation accuracy of the EnFCM, NDFCM, FLICM, and proposed IFF-FLICM is shown in Table 9. Further, to measure the segmentation performance, two quality measures, "structural similarity index (SSIM)

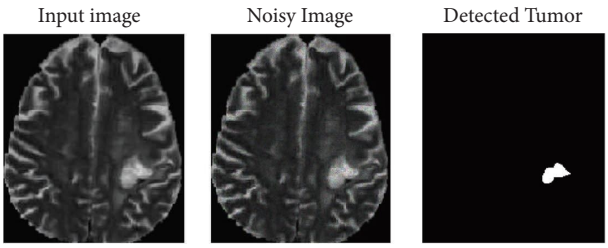

Figure 14: Segmentation of brain tumor using IFF-FLICM.

and peak signal-to-noise ratio (PSNR) [37]," are considered. The higher value of PSNR and SSIM represents good noise reduction capability. The proposed IFF-FLICM segmentation offered a PSNR value of 37.24 dB and an SSIM value of 0.9823, showing a good reduction of noise capability compared to the other mentioned EnFCM, NDFCM, and FLICM segmentation techniques. The values of SSIM and PSNR are presented in Table 10. The primary goal of segmentation is to identify and delineate regions of interest within an image. These regions correspond to tumor structures or other clinically relevant features. The segmentation output may be further annotated with clinically relevant information. For the purpose of comparison of segmentation techniques, we have taken the same image.

4.3. Results of IFF-FLICM Segmentation with Breast Cancer, BraTS, and COVID-19 Database. We have employed the IFF-FLICM segmentation on the Mini Mammographic Image Analysis Society (Mini-MIAS) [49], Digital Database for Mammography Screening (DDSM) [50], BraTS 2018 [46], BraTS 2019 [47], and COVID-19 [37] datasets. The performance results for different datasets are presented in Table 11. From Table 11, it is observed that the segmentation accuracy for breast cancer DDSM, Mini-MIAS, BraTS 2018, and BraTS 2019 achieved is nearly identical to the Dataset-255. However, the variations are observed in COVID-19 dataset due to the poor image quality. Also, SSIM and PSNR are higher, showing better segmentation. So the proposed IFF-FLICM outperforms the different datasets. Figure 15 shows the detection of the DDSM breast cancer dataset with IFF-FLICM segmentation. Figure 16 shows the Mini-MIAS breast cancer dataset, Figure 17 shows the COVID-19 dataset, Figure 18 shows BraTS 2018 brain tumor dataset, and Figure 19 shows the BraTS 2019 brain tumor dataset. It is observed that the proposed IFF-FLICM segmentation shows better segmentation results.

4.4. Classification Results. The comparison of training, testing, sensitivity, specificity, and computational time for PSO-ELM, MHS-ELM, SCA-ELM, and MHS-SCA-ELM models is presented in Table 6.

Table 6 shows the performance measure analysis of different classifiers along with the proposed MHS-SCA-ELM model. The performance measure analysis shows the uniqueness of the proposed MHS-SCA-ELM model. During training, the proposed MHS-SCA-ELM achieves 99.12% accuracy and 98.47% testing accuracy. This shows the performance improvement of the proposed model, as we know the model's authenticity is accepted based on the testing capability. Further, the sensitivity and specificity are 98.78% and 99.23%, respectively.

Table 10: Quality measures with Rician noise.

Algorithm	Rician noise	
	SSIM	PSNR (dB)
EnFCM	0.7324	23.17
NDFCM	0.8954	28.54
FLICM	0.9317	32.59
IFF-FLICM	**0.9823**	**37.24**

Table 11: Performance measure of IFF-FLICM segmentation with different datasets.

	IFF-FLICM segmentation		
Database	Accuracy (%)	SSIM	PSNR
DDSM	99.33	0.9818	37.18
Mini-MIAS	99.34	0.9811	37.13
COVID-19 dataset	98.82	0.9736	36.14
BraTS 2018	99.28	0.9817	37.19
BraTS 2019	99.31	0.9811	37.22
Dataset-255	99.37	0.9823	37.24

Figure 15: IFF-FLICM segmentation results of DDSM breast cancer dataset.

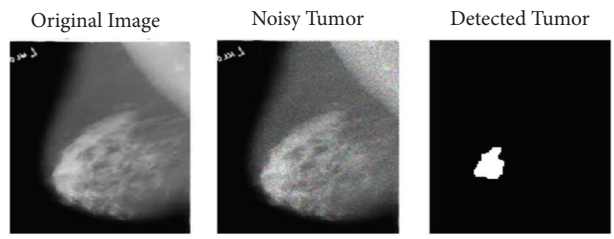

Figure 16: IFF-FLICM segmentation results of Mini-MIAS breast cancer dataset.

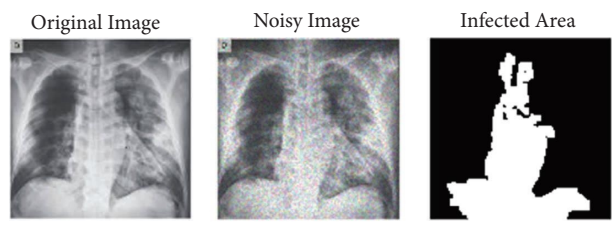

Figure 17: IFF-FLICM segmentation results of COVID-19 dataset.

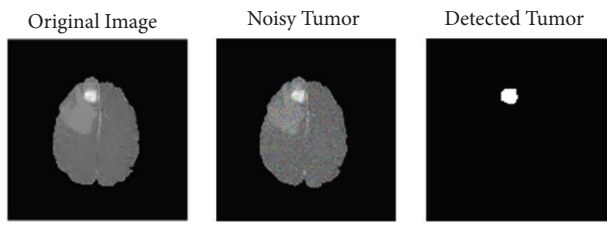

Figure 18: IFF-FLICM segmentation results of BraTS 2018 brain tumor dataset.

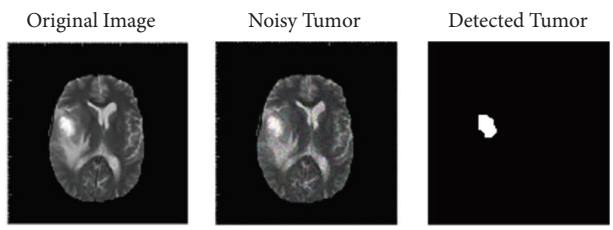

Figure 19: IFF-FLICM segmentation results of BraTS 2019 brain tumor dataset.

Computational time is important in the classification process for any new development model. The proposed MHS-SCA-ELM model took 23.2487 seconds, while the other mentioned models took more computational time for convergence.

The proposed model is tested with the 51 images of Dataset-255. Out of 51 images, 44 malignant and 7 benign images are considered for testing. One way to test the performance of the proposed model is to use cross-validation. Cross-validation involves partitioning the dataset into multiple subsets and using each subset as both training and testing data. We have taken 5×5 cross-validation. The data are partitioned into 5-folds, and each fold contains 51 images for a single run. There are five runs taken together, and then the average value of five runs is the average accuracy of the classification. Further, to test the performance of a proposed model, we can use metrics such as accuracy, precision, recall, and $F1$ score. Tables 12 and 13 show the 5×5 cross-validation procedure.

$$\begin{aligned} \text{Accuracy} &= \frac{(\text{TP} + \text{TN})}{(\text{TP} + \text{TN} + \text{FP} + \text{FN})}, \\ \text{Precision} &= \frac{\text{TP}}{(\text{TP} + \text{FP})}, \\ \text{Recall} &= \frac{\text{TP}}{(\text{TP} + \text{FN})}, \\ \text{F1 Score} &= \frac{2 * \text{Precision} * \text{Recall}}{(\text{Precision} + \text{Recall})}. \end{aligned} \tag{31}$$

The Fold-1 calculation is given by

$$\begin{aligned} \text{Performance metric} &= [\text{Accuracy Precision Recall } F1 \text{ Score}], \\ \text{Performance mertic} &= \begin{matrix} [0.9804 & 1.0000 & 0.9773 & 0.9885 \\ 1.0000 & 1.0000 & 1.0000 & 1.0000 \\ 1.0000 & 1.0000 & 1.0000 & 1.0000 \\ 1.0000 & 1.0000 & 1.0000 & 1.0000 \\ 0.9804 & 1.0000 & 0.9773 & 0.9885]. \end{matrix} \end{aligned} \tag{32}$$

The average value of column-4 represents the F1-Score, and the average value is obtained as 99.54%. All the values are obtained by taking the values of TP, TN, FN, and FP from Table 12. For each run, the performance metric is calculated and the average accuracy is achieved as 99.12%. For run-2, Accuracy (Column-1), Precision (Column-2), Recall (Column-3), and $F1$ Score (Column-4), values are obtained as 99.01%, 100%, 97.67%, and 98.83%, respectively. Similarly, we can calculate the values for Accuracy, Precision, Recall, and F1 score for each run.

The average values can be calculated as $=(0.9804 + 1 + 1 + 1 + 0.9844)/5 = 0.9921$ or 99.21%.

The proposed MHS-SCA-based ELM required around 570 iterations, whereas SCA-ELM, MHS-ELM, and PSO-ELM required about 600, 620, and 900 iterations, respectively, to converge as shown in Figure 20. The proposed MHS-SCA-based ELM takes 23.2487 seconds to compute, which is less than the computational times of the MHS-ELM, SCA-ELM, and PSO-ELM machine learning models. For the experiment, 1000 iterations are considered for each

Table 12: Cross-validation (5 × 5-fold Dataset-255) during run-1.

Fold	Test images	TP	FN	TN	FP	Accuracy (%)
1st fold	51	43	1	7	0	98.04
2nd fold	51	44	0	7	0	100
3rd fold	51	44	0	7	0	100
4th fold	51	44	0	7	0	100
5th fold	51	43	1	7	0	98.04
Final average accuracy						**99.21**

Table 13: Cross-validation (5 × 5-fold Dataset-255) for each run.

	1st fold	2nd fold	3rd fold	4th fold	5th fold	Total	Accuracy (%)
1st run	51	51	50	51	50	253	**99.21**
2nd run	51	51	50	50	50	252	98.82
3rd run	51	50	50	51	50	252	98.82
4th run	51	51	51	51	51	255	100
5th run	51	50	51	50	50	252	98.82
Final average accuracy							**99.12**

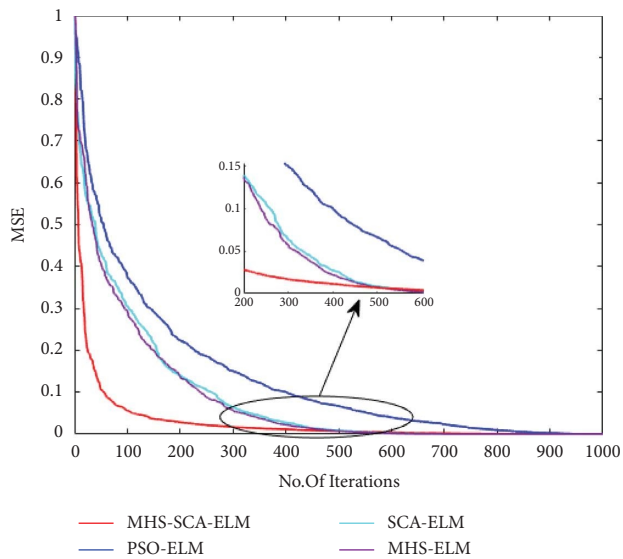

Figure 20: Mean square error results.

Table 14: Performance evaluation of different datasets.

Dataset	MHS-SCA-ELM		
	No. of iterations	Computational time (sec)	Accuracy (%)
DDSM	1000	25.1531	99.11
Mini-MIAS	1000	25.6112	99.10
COVID-19 dataset	1000	27.2457	98.86
BraTS 2018	1000	24.8957	99.11
BraTS 2019	1000	24.1245	99.12
Dataset-255 (proposed)	1000	23.2487	**99.12**

mentioned model. The performance evaluation results are presented in Table 6. The classification performance of different datasets is presented in Table 14.

The accuracy of the proposed MHS-SCA-ELM model is 99.12% with Dataset-255. The DDSM and Mini-MIAS breast cancer datasets achieved 99.11% accuracy and 99.10% accuracy which are nearly identical to the classification accuracy with Dataset-255. Also, the BraTS 2018 and BraTS 2019 brain tumor datasets achieved 99.11% accuracy and 99.12% accuracy. Also, the computational time is nearly similar in all the datasets except the COVID-19 dataset. The COVID-19 dataset achieved 98.86% accuracy due to poor image quality. It is observed from Table 14 that the proposed MHS-SCA-ELM model performs well in all the datasets mentioned. So the proposed MHS-SCA-ELM model shows its robustness in the classification of brain tumors.

5. Discussion

This study proposes an improved brain tumor detection and classification approach using a combination of fuzzy factor fuzzy local information C means segmentation and MHS-SCA optimized extreme learning machine. The proposed MHS-SCA optimization algorithm is employed for the weight optimization of the ELM model. The mathematical analysis for MHS-SCA optimization is developed by hybridizing SCA and harmony search algorithm. The pseudocode for MHS-SCA is presented in Table 2. The research implementation diagram is presented in Figure 1. MHS, SCA, PSO, and the proposed MHS-SCA for validating the proposed MHS-SCA optimized four multimodal functions and one unimodal benchmark function. The validation results are presented in Figure 5 for $F1$ function, Figure 6 for $F2$ function, Figure 7 for function $F3$, Figure 8 for $F4$ function, and Figure 9 for function $F5$. The clarity of the convergence for $F1$–$F5$ was also shown with a subfigure for distinguishing between the optimized graphs. The modified harmony search took a lesser number of iterations for convergence. There are 1000 iterations considered for the optimization of functions. Table 3 presents the benchmark functions utilized for the research, whereas Table 4 presents the pseudocode for MHS-SCA for weight optimization of the ELM model. Table 5 presents the parameters used for the simulation of MHS-SCA optimization algorithm. The Dataset-255 details are presented in Table 7. The benchmark functions' optimal values for PSO, SCA, MHS, and MHS-SCA are presented in Table 8. Figure 10 presents the optimal value comparison for functions $F1$–$F5$. The brain tumor images underwent IFF-FLICM segmentation and Mexican wavelet transform feature extraction. The mathematical analysis for IFF-FLICM segmentation was developed and presented. Figure 11 presents the EnFCM segmentation with higher noise content, and Figure 12 shows the segmentation of tumors using NDFCM. The FLICM segmentation is shown in Figure 13. The proposed IFF-FLICM segmentation with noise reduction is shown in Figure 14. Table 9 shows the segmentation accuracy of the EnFCM, NDFCM, FLICM, and proposed IFF-FLICM segmentation techniques. The quality measures SSIM and PSNR are presented in Table 10. The performance measures, accuracy, specificity, and sensitivity of the classifiers PSO-ELM, MHS-ELM, SCA-ELM, and MHS-SCA-ELM are presented in Table 11. Table 6 shows the classification performance of the models. Figure 13 shows the mean square results of PSO-ELM, MHS-ELM, SCA-ELM, and MHS-SCA-ELM classifier models. The proposed model MHS-SCA-ELM is unique in classifying benign and malignant brain tumors. The proposed MHS-SCA-ELM model's accuracy performance is compared with previous research and presented in Table 15. Tables 12 and 13 show the 5×5 cross-validation procedure for each fold and run during training. Table 14 shows the classification accuracy of the breast cancer, BraTS 2018, BraTS 2019, and COVID-19 datasets. We have consulted the Adama General Hospital, Adama, Ethiopia, and shown them the results of our model, and they suggested for prototype design. The prototype development using embedded platform is our future research work. Figures 21 and 22 show the Dataset-255 images and IFF-FLICM segmentation results.

The MHS-SCA-ELM model is a hybrid algorithm that combines the optimization capabilities of the modified harmony search algorithm and sine cosine algorithm with the fast learning speed of extreme learning machine (ELM) for classification tasks to avoid overfitting. Generally, ELM models are considered less interpretable than traditional machine learning models because the weights assigned to each input feature are randomly generated, and the model needs to explain how these weights are determined. Furthermore, the lack of insight into the model's superiority could indicate that the model needs to be more balanced with the training data. Overfitting occurs when a model is overly intricate and matches the noise in the training data instead of the underlying patterns. As a result, the model may perform well on the training set of data. The MHS and SCA algorithms were used separately to optimize the weights in order to improve the performance of the ELM model, and the results are displayed in Table 6 with classification accuracy values that are lower than those of the prior research. By incorporating MHS-SCA weight optimization process that aims to minimize the sum of the squared errors between the predicted and actual outputs, this process helps to identify the optimal weights for each input feature and allows for greater interpretability of the model. During the processing of training, the weights are randomly generated for the purpose of optimization. The position equations of the sine cosine algorithm are mapped into the weight vectors. In the MHS-SCA, the parameters of SCA played an important role in convergence. Also, the learning parameter and pitch adjustment of harmonic search improve the weight optimization process to achieve better classification efficiency. According to the controlling parameter variation, the sine and cosine functions change their position to an updated position. Along with that, the weights also changed their values from the old weight values to new weight values. This process will continue till the optimal values of weights are achieved. From the comparison of data provided in

Table 15: Comparison of previous research with proposed model.

Author	Classifier	Dataset used	Accuracy (%)
Varuna Shree and Kumar [51]	Probabilistic neural network (PNN)	650 MR images	95
Rajan and Sundar [52]	Support vector machine (SVM)	41 magnetic resonance (MR) images	98
Ullah et al. [53]	Feed-forward neural network	71 magnetic resonance (MR) images	95.8
Kang et al. [54]	ELM	253 images	97.05
Díaz-Pernas et al. [55]	Multiscale CNN	3064 MR images	97.3
Our proposed method	MHS-SCA-ELM	255 images	99.12

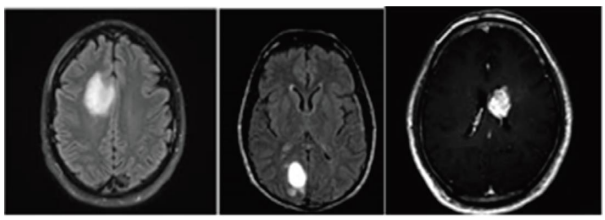

Figure 21: Dataset-255 images.

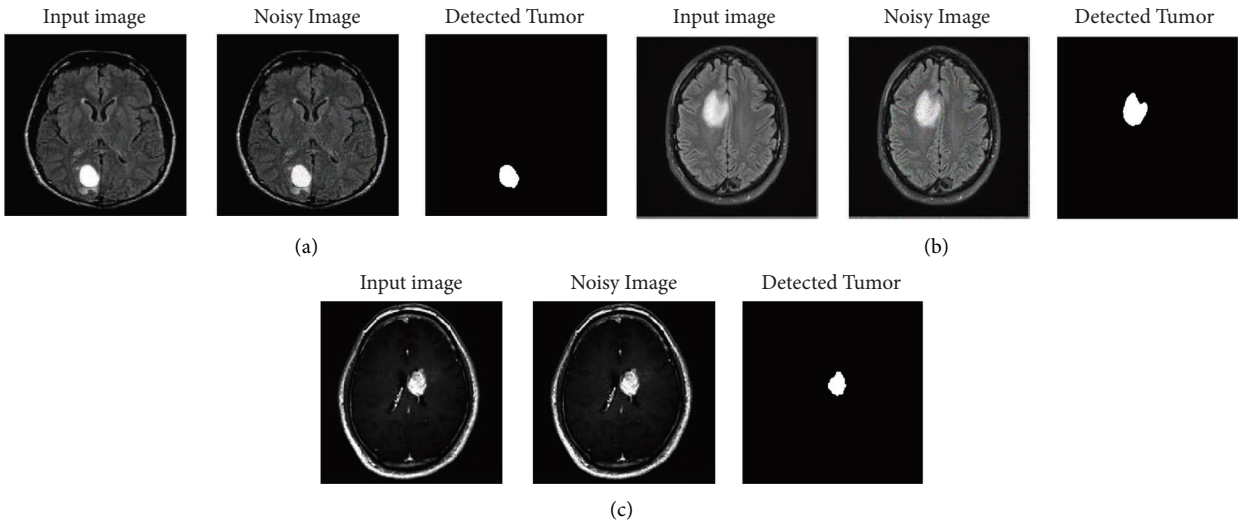

Figure 22: (a–c) IFF-FLICM segmentation results of Dataset-255.

Table 8, it is observed that the work proposed by Kang et al. [49], with 253 images, obtained a 97.05% accuracy for the ELM model. Díaz-Pernas et al. [50] acquired 97.3% accuracy in conjunction with the multiscale CNN classifier with a dataset of 3064 images. We, however, obtain better accuracy of 99.12% for the Dataset-255 using MHS-SCA in combination with ELM as the classifier. This proves that the proposed MHS-SCA, combined with the ELM classifier, achieved good performance compared to other algorithms.

5.1. Advantages of Proposed IFF-FLICM Segmentation and MHS-SCA-ELM Model. The improved fuzzy factor fuzzy local information C means (IFF-FLICM) segmentation is a valuable technique in the field of medical imaging, particularly for brain tumor analysis, where accuracy, complexity, and clinical significance are important. The advantages are mentioned below:

(i) Improved FF-FLICM algorithms can enhance the accuracy of brain tumor segmentation results compared to traditional methods. The IFF-FLICM algorithm influences fuzzy logic and local information to capture subtle variations in tumor boundaries, which can be challenging for other segmentation techniques.

(ii) By incorporating local contextual information, improved FF-FLICM can reduce segmentation errors and enhance image quality, intensity, and contrast, leading to more reliable and clinically meaningful results.

(iii) Improved FF-FLICM can reduce the need for manual segmentation efforts, saving time for radiologists and clinicians while maintaining segmentation quality. It will provide a platform for researchers to explore novel segmentation

techniques and incorporate domain-specific knowledge to improve brain tumor analysis. It can be integrated into clinical analysis to facilitate seamless use by healthcare professionals.

The hybridization of MHS and SCA offers a potent method to optimize ELM weights in the context of classifying images of brain tumors, increasing accuracy, robustness, and effectiveness. However, it is crucial to verify the significance of this hybridization through proper parameter adjusting. The following are the advantages:

(i) The hybrid MHS-SCA-ELM model helps achieve higher classification accuracy and prevents overfitting of brain tumor images, which is crucial for accurate diagnosis and treatment development.

(ii) Combining the strengths of both MHS and SCA, we obtained optimal solutions more quickly. As the optimization progresses, the MHS-SCA component fine-tuned the weights locally, leading to faster convergence to an optimal solution.

(iii) As brain tumor images have complex and noisy features, the hybrid approach improves the robustness of the optimization process by mitigating the risk of getting stuck in local optima and by adapting to the diverse characteristics of the image data.

(iv) The hybridization of MHS and SCA leads to more consistent and stable optimization results across different brain tumor and other medical image datasets, which shows confidence in the model's performance.

5.2. Limitations and Future Work Recommendations. The improved FF-FLICM algorithm can also be applied to handle noisy pixels of the brain tumor more effectively by modifying the membership function further. Adaptively adjusting the weighting of local information based on the characteristics of the image can help the algorithm perform better in regions with varying levels of detail and contrast. IFF-FLICM algorithm can also be applied in medical imaging and other domains where multiple sources of information need to be fused for segmentation. The IFF-FLICM algorithm allows users, such as radiologists or image analysts, to provide feedback to guide the segmentation process. This can improve the accuracy of segmentation results and make the algorithm more user-friendly. The IFF-FLICM technique can be involved as a preprocessing step in deep learning models such as convolutional neural networks (CNNs) or recurrent neural networks (RNNs) to enhance the representational power of deep neural networks.

The hybrid MHS-SCA optimization technique can be used to fine-tune pretrained ELM models on a smaller, domain-specific dataset to improve generalization for brain tumor classification tasks. By deploying optimized MHS-SCA-ELM model inference on hardware platforms in real-time clinical settings, the mortality rate due to brain tumor disease can be avoided at an early stage. In collaboration with medical professionals, the performance of the hybrid ELM model on diverse and large-scale clinical datasets can meet the standards required for clinical applications. The optimized MHS-SCA-ELM models can be taken into decision support systems for radiologists to ensure user-friendly interfaces that enable medical practitioners to interact with the model's predictions and recommendations effectively. The hybrid MHS-SCA optimization approach can be adapted for transfer learning scenarios. The MHS-SCA optimization can be integrated with k-NN and SVM models [56]. The proposed MHS-SCA-ELM model is robust and unique due to its accuracy and computational time. The proposed model is validated for breast cancer, COVID-19 datasets, etc., but not for the larger image datasets.

These future directions can significantly advance the application of hybridized optimization techniques for brain tumor image classification using ELM models, ultimately leading to more accurate, efficient, and clinically valuable tools for medical practitioners and researchers.

6. Conclusion

In this research, IFF-FLICM segmentation was proposed for segmenting brain tumors. The proposed approach enhances the accuracy and reliability of tumor segmentation by incorporating a fuzzy factor in the clustering process to handle uncertainties in medical imaging. Additionally, the local information of each pixel is considered to improve the performance, resulting in a more detailed segmentation of the tumor. The proposed IFF-FLICM segmentation shows good capability in reducing noise and tumor extraction from the MRI images. The Mexican hat wavelet was applied for feature extraction of the segmented images. A hybrid modified harmony search-sine cosine algorithm (MHS-SCA) algorithm was proposed for weight optimization of the ELM model to enhance the performance of the ELM model. Five benchmark functions were considered to show the proposed MHS-SCA optimization algorithm's effectiveness. The proposed MHS-SCA optimized the benchmark functions and was compared with PSO, MHS, and SCA optimization algorithms to show the robustness of the MHS-SCA. The optimal values for functions ($F1$–$F5$) of the proposed MHS-SCA show the uniqueness of the algorithm. The MHS-SCA optimized extreme learning machine was then employed to classify the segmented tumor into cancerous or noncancerous categories. The Harvard Medical School dataset was utilized for the training and testing process. The training and testing data were fed to the proposed MHS-SCA-ELM model for brain tumor classification. The other models, such as PSO-ELM, MHS-ELM, and SCA-ELM, were also considered for the classification of brain tumors, and results from the models were compared with the proposed MHS-SCA-ELM model. The proposed MHS-SCA-based ELM model achieved an accuracy of 99.12% classification. Also, a sensitivity, specificity, and accuracy of 98.78%, 99.23%, and 99.12% and a computational time of 23.2478 seconds were achieved. Similarly, the proposed model achieves precision of 99.29%, recall of

98.21%, and $F1$ score of 99.72%. The segmentation and classification results for breast cancer and COVID-19 datasets are presented in Tables 11 and 14 to show the authenticity of the IFF-FLICM segmentation and MHS-SCA-ELM model. The proposed MHS-SCA can also be applied for weight optimization of other machine learning models for different medical image classifications. The experimental results demonstrate that the proposed MHS-SCA-ELM approach outperforms the PSO-ELM, MHS-ELM, and SCA-ELM methods in terms of accuracy, sensitivity, specificity, and computational time. The proposed MHS-SCA-ELM classifier has the potential to aid radiologists in accurately detecting and classifying brain tumors, leading to better diagnosis and treatment planning.

Data Availability

The data have been collected from the Medical School of Harvard University and will be provided upon request to the corresponding author.

Conflicts of Interest

The authors declare that they have no conflicts of interest.

References

[1] H. Win, R. Krishnappa, and Y. Deol, "Psychosis as primary presentation of brain tumor: a case report," *American Journal of Geriatric Psychiatry*, vol. 29, no. 4, pp. S97–S98, 2021.

[2] L. Szilagyi, Z. Benyo, S. M. Szilagyii, and H. S. Adam, "MR brain image segmentation using an enhanced fuzzy c-means algorithm," in *Proceeding of the 25th Annual International Conference of the IEEE EMBS*, pp. 17–21, Cancun, Mexico, September 2003.

[3] W. Cai, S. Chen, and D. Zhang, "Fast and robust fuzzy c-means clustering algorithms incorporating local information for image segmentation," *Pattern Recognition*, vol. 40, no. 3, pp. 825–838, 2007.

[4] L. Abualigah, A. Diabat, and Z. W. Geem, "A comprehensive survey of the harmony search algorithm in clustering applications," *Applied Sciences*, vol. 10, no. 11, p. 3827, 2020.

[5] L. Wang, R. Yang, Y. Xu, Q. Niu, P. M. Pardalos, and M. Fei, "An improved adaptive binary Harmony Search algorithm," *Information Sciences*, vol. 232, pp. 58–87, 2013.

[6] R. Sarkhel, N. Das, A. Saha, and M. Nasipuri, "An improved Harmony Search Algorithm embedded with a novel piecewise opposition based learning algorithm," *Engineering Applications of Artificial Intelligence*, vol. 67, pp. 317–330, 2018.

[7] F. Valdez and C. Peraza, "Dynamic parameter adaptation in the harmony search algorithm for the optimization of interval type-2 fuzzy logic controllers," *Soft Computing*, vol. 24, no. 1, pp. 179–192, 2020.

[8] H. B. Ouyang, L. Gao, S. Li, X. Y. Kong, Q. Wang, and D. Zou, "Improved harmony search algorithm: lhs," *Applied Soft Computing*, vol. 53, pp. 133–167, 2017.

[9] N. M. Bala and S. B. Safei, "Hybrid harmony search and particle swarm optimization algorithm (HSPSO) for testing non-functional properties in software system stat," *Statistics, Optimization and Information Computing*, vol. 10, pp. 968–982, 2022.

[10] T. Lei, X. Jia, Y. Zhang, L. He, H. Meng, and A. K. Nandi, "Significantly fast and robust fuzzy c-means clustering algorithm based on morphological reconstruction and membership filtering," *IEEE Transactions on Fuzzy Systems*, vol. 26, no. 5, pp. 3027–3041, 2018.

[11] J. Amin, M. Sharif, M. Raza, T. Saba, and A. Rehman, "Brain tumor classification: feature fusion," in *Proceeding of the 2019 International Conference on Computer and Information Sciences (ICCIS)*, pp. 1–6, Sakaka, Saudi Arabia, June 2019.

[12] M. Nazir, M. A. Khan, T. Saba, and A. Rehman, "Brain tumor detection from MRI images using multi-level wavelets," in *Proceeding of the 2019 International Conference on Computer and Information Sciences (ICCIS)*, pp. 1–5, Sakaka, Saudi Arabia, June 2019.

[13] T. Saba, A. Rehman, M. N. Shahzad, R. Latif, S. A. Bahaj, and J. Alyami, "Machine learning for post-traumatic stress disorder identification utilizing resting-state functional magnetic resonance imaging," *Microscopy Research and Technique*, vol. 85, no. 6, pp. 2083–2094, 2022.

[14] B. Badjie and E. Deniz Ülker, "A deep transfer learning based architecture for brain tumor classification using MR images," *Information Technology and Control*, vol. 51, no. 2, pp. 332–344, 2022.

[15] S. Z. Kurdi, M. H. Ali, M. M. Jaber, T. Saba, A. Rehman, and R. Damaševičius, "Brain tumor classification using meta-heuristic optimized convolutional neural networks," *Journal of Personalized Medicine*, vol. 13, no. 2, p. 181, 2023.

[16] S. Maqsood, R. Damaševičius, and R. Maskeliūnas, "Multi-modal brain tumor detection using deep neural network and multiclass SVM," *Medicina*, vol. 58, no. 8, p. 1090, 2022.

[17] V. Rajinikanth, S. Kadry, R. Damaševičius, R. A. Sujitha, G. Balaji, and M. A. Mohammed, "Glioma/glioblastoma detection in brain MRI using pre-trained deep-learning scheme," in *Proceeding of the 2022 Third International Conference on Intelligent Computing Instrumentation and Control Technologies (ICICICT)*, pp. 987–990, Kannur, India, July 2022.

[18] V. Annepu, D. R. Sona, C. Ravikumar et al., "Review on unmanned aerial vehicle assisted sensor node localization in wireless networks: soft computing approaches," *IEEE Access*, vol. 10, pp. 132875–132894, 2022.

[19] V. Annepu and R. Anbazhagan, "Implementation of an efficient extreme learning machine for node localization in unmanned aerial vehicle assisted wireless sensor networks," *International Journal of Communication Systems*, vol. 33, no. 10, p. e4173, 2020.

[20] R. K. Patel and M. Kashyap, "Automated diagnosis of COVID stages from lung CT images using statistical features in 2-dimensional flexible analytic wavelet transform," *Biocybernetics and Biomedical Engineering*, vol. 42, no. 3, pp. 829–841, 2022.

[21] R. K. Patel and M. Kashyap, "Automated diagnosis of COVID stages using texture-based Gabor features in variational mode decomposition from CT images," *International Journal of Imaging Systems and Technology*, vol. 33, no. 3, pp. 807–821, 2023.

[22] R. K. Patel and M. Kashyap, "Machine learning- based lung disease diagnosis from CT images using Gabor features in Littlewood Paley empirical wavelet transform (LPEWT) and LLE," *Computer Methods in Biomechanics and Biomedical Engineering: Imaging and Visualization*, vol. 11, no. 5, pp. 1762–1776, 2023.

[23] R. K. Patel and M. Kashyap, "Automated screening of glaucoma stages from retinal fundus images using BPS and

LBP based GLCM features," *International Journal of Imaging Systems and Technology*, vol. 33, no. 1, pp. 246–261, 2023.

[24] R. Singh, A. Goel, and D. K. Raghuvanshi, "Computer-aided diagnostic network for brain tumor classification employing modulated Gabor filter banks," *The Visual Computer*, vol. 37, no. 8, pp. 2157–2171, 2021.

[25] S. A. Qureshi, S. E. A. Raza, L. Hussain et al., "Intelligent ultra-light deep learning model for multi-class brain tumor detection," *Applied Sciences*, vol. 12, no. 8, p. 3715, 2022.

[26] B. Shi, Q. Wang, S. Yin, Z. Yue, Y. Huai, and J. Wang, "A binary harmony search algorithm as channel selection method for motor imagery-based BCI," *Neurocomputing*, vol. 443, pp. 12–25, 2021.

[27] L. V. Enikeeva, E. N. Shvareva, and I. M. Gubaydullin, "Gravitational search and harmony search algorithms for solving the chemical kinetics optimization problems," *Engineering Journal*, vol. 25, no. 6, pp. 107–121, 2021.

[28] S. Daliri, "Using harmony search algorithm in neural networks to improve fraud detection in banking system," *Computational Intelligence and Neuroscience*, vol. 2020, Article ID 6503459, pp. 1–5, 2020.

[29] Q. Zhu, X. Tang, and A. Elahi, "Automatic clustering based on dynamic parameters harmony search optimization algorithm," *Pattern Analysis and Applications*, vol. 25, no. 4, pp. 693–709, 2022.

[30] M. A. Al-Betar, M. A. Awadallah, A. T. Khader, and Z. A. Abdalkareem, "Island-based harmony search for optimization problems," *Expert Systems with Applications*, vol. 42, no. 4, pp. 2026–2035, 2015.

[31] A. K. Al-Shamiri, A. Sadollah, and J. H. Kim, "Harmony search algorithms for optimizing extreme learning machines, proceedings of 6th international conference on harmony search, soft computing and applications," *Advances in Intelligent Systems and Computing*, vol. 1275, 2022.

[32] X. Dai, X. Yuan, and Z. Zhang, "A self-adaptive multi-objective harmony search algorithm based on harmony memory variance," *Applied Soft Computing*, vol. 35, pp. 541–557, 2015.

[33] S. S. Haghshenas, S. S. Haghshenas, Z. W. Geem et al., "Application of harmony search algorithm to slope stability analysis," *Land*, vol. 10, no. 11, p. 1250, 2021.

[34] N. F. Mansor, Z. A. Abas, A. S. Shibghatullah, and A. F. N. A. Rahman, "Modified parameters of harmony search algorithm for better searching," *IOP Conference Series: Materials Science and Engineering*, vol. 226, Article ID 012113, 2017.

[35] M. A. Al-Betar, "Island-based harmony search algorithm for non-convex economic load dispatch problems," *Journal of Electrical Engineering and Technology*, vol. 16, no. 4, pp. 1985–2015, 2021.

[36] A. Al-Shaikh, B. A. Mahafzah, and M. Alshraideh, "Retracted article: hybrid harmony search algorithm for social network contact tracing of COVID-19," *Soft Computing*, vol. 27, no. 6, pp. 3343–3365, 2021.

[37] S. Mishra, D. J. Gelmecha, R. S. Singh, D. S. Rathee, and T. Gopikrishna, "Hybrid WCA–SCA and modified FRFCM technique for enhancement and segmentation of brain tumor from magnetic resonance images," *Biomedical Engineering: Applications, Basis and Communications*, vol. 33, no. 3, Article ID 2150017, 2021.

[38] M. Seyedali, "SCA: a sine cosine algorithm for solving optimization problems," *Knowledge-Based Systems*, vol. 96, 2016.

[39] S. Mishra, P. Sahu, and M. R. Senapati, "MASCA- PSO based LLRBFNN model and improved fast and robust FCM algorithm for detection and classification of brain tumor from MR image," *Evolutionary Intelligence*, vol. 12, no. 4, pp. 647–663, 2019.

[40] X. Z. Gao, V. Govindasamy, H. Xu, X. Wang, and K. Zenger, "Harmony search method: theory and applications," *Computational Intelligence and Neuroscience*, vol. 2015, Article ID 258491, pp. 1–10, 2015.

[41] S. Panda, S. Mishra, and M. N. Mohanty, "Epliptic brain tumor detection and classification using cumulative sum average filter TT-transform and harmony search algorithm based LLRBFN model," *PalArch's Journal of Archaeology of Egypt/Egyptology*, vol. 17, no. 9, pp. 2329–2339, 2020.

[42] S. Panda, S. Mishra, M. N. Mohanty, and S. Satapathy, "Epileptic seizure classification using adaptive sine cosine algorithm-whale optimization algorithm optimized learning machine model," in *Proceedings of the 2023 International Conference in Advances in Power, Signal, and Information Technology (APSIT)*, pp. 1–5, Bhubaneswar, India, August 2023.

[43] I. S. Samanta, P. K. Rout, K. Swain, M. Cherukuri, and S. Mishra, "Power quality events recognition using enhanced empirical mode decomposition and optimized extreme learning machine," *Computers and Electrical Engineering*, vol. 100, Article ID 107926, 2022.

[44] I. S. Samanta, P. K. Rout, and S. Mishra, "An optimal extreme learning-based classification method for power quality events using fractional Fourier transform," *Neural Computing and Applications*, vol. 33, no. 10, pp. 4979–4995, 2021.

[45] S. Krinidis and V. Chatzis, "A robust fuzzy local information cmeans clustering algorithm," *IEEE Transactions on Image Processing*, vol. 19, no. 5, pp. 1328–1337, 2010.

[46] J. Nalepa, P. Ribalta Lorenzo, M. Marcinkiewicz et al., "Fully-automated deep learning-powered system for DCE-MRI analysis of brain tumors," *Artificial Intelligence in Medicine*, vol. 102, Article ID 101769, 2020.

[47] K. Ben Ahmed, L. O. Hall, D. B. Goldgof, and R. Gatenby, "Ensembles of convolutional neural networks for survival time estimation of high-grade glioma patients from multimodal MRI," *Diagnostics*, vol. 12, no. 2, p. 345, 2022.

[48] V. Mudeng, M. Kim, and S. W. Choe, "Prospects of structural similarity index for medical image analysis," *Applied Sciences*, vol. 12, no. 8, p. 3754, 2022.

[49] J. P. Suckling, "The mammographic image analysis society digital mammogram database exerpta medica," *International Congress Series*, vol. 1069, pp. 375–378, 1994.

[50] M. Heath, K. Bowyer, D. Kopans et al., "The digital database for screening mammography," in *Fifth International Workshop on Digital Mammography*, M. J. Yaffe, Ed., pp. 212–218, Medical Physics Publishing, Madison, WI, USA, 2001.

[51] N. Varuna Shree and T. N. R. Kumar, "Identification and classification of brain tumor MRI images with feature extraction using DWT and probabilistic neural network," *Brain Informatics*, vol. 5, no. 1, pp. 23–30, 2018.

[52] P. G. Rajan and C. Sundar, "Brain tumor detection and segmentation by intensity adjustment," *Journal of Medical Systems*, vol. 43, no. 8, pp. 282–313, 2019.

[53] Z. Ullah, M. U. Farooq, S. H. Lee, and D. An, "A hybrid image enhancement based brain MRI images classification technique," *Medical Hypotheses*, vol. 143, Article ID 109922, 2020.
[54] J. Kang, Z. Ullah, and J. Gwak, "MRI-based brain tumor classification using ensemble of deep features and machine learning classifiers," *Sensors*, vol. 21, no. 6, p. 2222, 2021.
[55] F. J. Díaz-Pernas, M. Martínez-Zarzuela, M. Antón-Rodríguez, and D. González-Ortega, "A deep learning approach for brain tumor classification and segmentation using a Multiscale convolutional neural network," *Healthcare*, vol. 9, no. 2, p. 153, 2021.
[56] S. A. Qureshi, L. Hussain, U. Ibrar et al., "Radiogenomic classification for MGMT promoter methylation status using multi-omics fused feature space for least invasive diagnosis through mpMRI scans," *Scientific Reports*, vol. 13, no. 1, p. 3291, 2023.